A global marine particle size distribution dataset obtained with the Underwater Vision Profiler 5

Rainer Kiko[1,*], Marc Picheral[1,*], David Antoine[2,1], Marcel Babin[3], Léo Berline[4], Tristan Biard[5], Emmanuel Boss[6], Peter Brandt[7,8], Francois Carlotti[4], Svenja Christiansen[9], Laurent Coppola[1], Leandro de la Cruz[10], Emilie Diamond-Riquier[1], Xavier Durrieu de Madron[11], Amanda Elineau[12], Gabriel Gorsky[1], Lionel Guidi[1], Helena Hauss[7], Jean-Olivier Irisson[1], Lee Karp-Boss[6], Johannes Karstensen[7], Dong-gyun Kim[13], Rachel M. Lekanoff[14], Fabien Lombard[1], Rubens M. Lopes[10], Claudie Marec[3], Andrew M.P. McDonnell[14], Daniela Niemeyer[7], Margaux Noyon[15], Stephanie H. O'Daly[14], Mark Ohman[16], Jessica L. Pretty[14], Andreas Rogge[17,13], Sarah Searson[18], Masashi Shibata[19], Yuji Tanaka[20], Toste Tanhua[7], Jan Taucher[7], Emilia Trudnowska[21], Jessica S. Turner[22], Anya Waite[23], and Lars Stemmann[1]

[1]Sorbonne Université, CNRS, UMR 7093, Laboratoire d'Océanographie de Villefranche-sur-Mer (LOV), Villefranche-sur-Mer, France
[2]Remote Sensing and Satellite Research Group, School of Earth and Planetary Sciences, Curtin University, Perth, WA 6845, Australia
[3]Département de Biologie, Université Laval, Québec, Canada
[4]MIO, Aix Marseille Univ., Université de Toulon, CNRS, IRD, MIO, Marseille, France UMR 7294 Mediterranean Institute of Oceanography, Marseille, France
[5]Univ. Littoral Côte d'Opale, Univ. Lille, CNRS, UMR 8187 - LOG - Laboratoire d'Océanologie et de Géosciences, F-62930 Wimereux, France
[6]School of Marine sciences, University of Maine, Orono, Massachusetts, USA
[7]GEOMAR Helmholtz Centre for Ocean Research Kiel, Kiel, Germany
[8]Faculty of Mathematics and Natural Sciences, Kiel University, Kiel, Germany
[9]Department of Biosciences, University of Oslo, Oslo, Norway
[10]University of São Paulo, Oceanographic Institute, São Paulo, Brazil
[11]CEFREM, CNRS-Université de Perpignan Via Domitia, Perpignan, France
[12]Institut de la Mer de Villefranche, CNRS - Sorbonne Université, Villefranche-sur-Mer, FRANCE
[13]Alfred-Wegener-Institut Helmholtz-Zentrum für Polar- und Meeresforschung, Bremerhaven, Germany
[14]College of Fisheries and Ocean Sciences, University of Alaska Fairbanks, Fairbanks, Alaska, USA
[15]Nelson Mandela University, Institute for Coastal and Marine Research, Gqeberha, South Africa
[16]Scripps Institution of Oceanography, La Jolla, California, USA
[17]Institute for Ecosystem Research, Kiel University, Kiel, Germany
[18]National Institute of Water and Atmosphere Research, New Zealand
[19]SeaBreath Co., Ltd., Tokyo, Japan
[20]Tokyo University of Marine Science and Technology, Tokyo, Japan
[21]Department of Marine Ecology, Institute of Oceanology Polish Academy of Sciences, Sopot, Poland
[22]Department of Marine Sciences, University of Connecticut Avery Point, Groton, Connecticut, USA
[23]Dalhousie University, Halifax, Nova Scotia, Canada
[*]These authors contributed equally to this work.

Correspondence: Rainer Kiko (rainer.kiko@obs-vlfr.fr)

Abstract. Marine particles of different nature are found throughout the global Ocean. The term "marine particles" describes detritus aggregates, fecal pellets, but also bacterio-, phyto-, zooplankton and nekton. Here we present a global particle size distribution dataset obtained with several Underwater Vision Profiler 5 (UVP5) camera systems. Overall, within the 64 μm to about 50 mm size range covered by the UVP5, detrital particles are the most abundant component of all marine particles in this size range and thus measurements of the particle size distribution with the UVP5 can yield important information on detrital particle dynamics. During deployment, which is possible down to 6000 m depth, the UVP5 images a volume of about 1 L at a frequency of 6 to 20 Hz. Each image is segmented in real time and size measurements of particles are automatically stored. All UVP5 units used to generate the here presented dataset were inter-calibrated using a UVP5 High Definition unit as reference. Our consistent particle size distribution dataset contains 8805 vertical profiles collected between 2008-06-19 and 2020-11-23. All major ocean basins, as well as the Mediterranean and the Baltic Sea were sampled. 19% of all profiles had a maximum sampling depth shallower than 200 dbar, 38% sampled at least the upper 1000 dbar depth range and 11% went down to at least 3000 dbar depth. First analysis of the particle size distribution dataset shows that particle abundance is found to be high at high latitudes and in coastal areas where surface productivity or continental inputs are elevated. Lowest values are found in the deep ocean and in the oceanic gyres. Our dataset should be valuable for more in-depth studies that focus on the analysis of regional, temporal and global patterns of particle size distribution and flux as well as for the development and adjustment of regional and global biogeochemical models. The marine particle size distribution dataset (Kiko et al., 2021) is available at https://doi.pangaea.de/10.1594/PANGAEA.924375.

1 Introduction

1.1 Nature and origin of marine particles

Bacterio-, phyto- and zooplankton, nekton, aggregates, marine snow, fecal pellets, biomineralized shells, mineral dust, precipitates, suspended clay and nowadays also plastics are part of the general marine particle size spectrum (Sheldon and Parsons, 1967; Stemmann and Boss, 2012; Cózar et al., 2014). The relative contribution of living particles to the total load of particles is not well known and may vary according to the particle size range and the marine ecosystem investigated from 1% to 50% (Forest et al., 2012; Stemmann and Boss, 2012; Checkley Jr et al., 2008). Abiotic particles can originate from resuspension at the seabed (Puig et al., 2013; McCave, 2009, 1986; Honjo et al., 1984), dust deposition (Zuniga et al., 2008; Ratmeyer et al., 1999) and influx by rivers (Ludwig and Probst, 1998) and glaciers (Neal et al., 2010). Furthermore, dissolved constituents precipitate when riverwater (Many et al., 2019) or hydrothermal fluids (German and Von Damm, 2003) mix with seawater. Photosynthesis by planktonic algae is the almost exclusive source of biogenic carbon in the open ocean, although other processes such as carbon fixation by chemoautotrophs, benthic algae, seagrass and, moreover, land and river derived organic particles add to this as well (see e.g. (Duarte et al., 2010; Ludwig and Probst, 1998)). Higher trophic levels consume this biogenic carbon to build up biomass and fuel physiological activity. Along the entire plankton trophic web, part of the consumed carbon is also transformed into detritus (fecal pellets, exuviae, discarded houses or dead bodies). Small particles such as phytoplankton cells can also coagulate to form larger aggregates, that might also include other detrital particles (Jackson, 1990). The two pathways lead

to the formation of detrital particles, with different sinking properties depending on their size, content and porosity (Stemmann et al., 2004). As particle size is an essential trait for many biotic and abiotic interactions, it is often used to develop and calibrate size resolved mechanistic models of phytoplankton bloom formation, particle coagulation and export to the mesopelagic zone (Stemmann et al., 2004; Jouandet et al., 2014; Bianchi et al., 2018). Moreover, the size structure of particles and plankton is one of the most relevant indicators of ecosystem functionality and energy fluxes (Jackson, 1990; Zhou; Stemmann and Boss, 2012). How abiotic and biotic marine particles of different sizes are formed, destroyed, advected or sink are key questions in ocean carbon cycling and biogeochemistry (Stemmann et al., 2012; Boyd et al.; Giering et al., 2020) and therefore their quantitative monitoring is needed.

1.2 Marine particle imaging

Many phyto- and zooplankton organisms, but also some other particles are sturdy and can be sampled using nets, traps, sediment traps, bottles and in situ filtration devices. Fragile particles often formed by aggregation of diverse source particles (dead cells, fecal pellets, exudates, minerals) called "Marine snow" (Beebe, 1931) and fragile zooplankton such as cnidarians, rhizarians and other gelatinous organisms are however not amenable to such sampling methods (O'Hern et al.; Alldredge and Silver, 1988; Wiebe and Benfield, 2003; Remsen et al., 2004). Therefore, only in situ measurements allow for a realistic assessment of the size and abundance of marine particles (Alldredge and Silver, 1988). Earliest such measurements were made from moored platforms, submersibles or by divers and included analyses of photographic images (Suzuki and Kato, 1953; Alldredge and Gotschalk, 1988). Advancement in electronic components and digital processing routines then allowed for the development of instruments such as the optical plankton counter (Herman, 1992), holographic instruments (Katz et al., 1999) and various camera systems (Asper, 1987; Honjo et al., 1984; Lampitt et al., 1993; Ratmeyer and Wefer, 1996; Benfield et al., 2007). Among them the Underwater Vision Profiler (UVP) (Gorsky et al., 2000; Picheral et al., 2010) was designed to automatically size and count undisturbed abiotic and biotic marine particles.

1.3 The Underwater Vision Profiler and its use

The UVP was developed at the Laboratoire d'Océanographie de Villefranche (LOV) to provide consistent measurements of particle abundance and size. Single units of UVP versions 1 to 4 were produced from 1991 to 2008 (Gorsky et al., 2000, 2002). The first prototype (sn000) of version 5 started field operations in 2008 and was described in detail by Picheral et al. (2010). The instrument was commercialised in 2010 and produced until 2021. A standard (STD) version with a 1.3 Megapixel greyscale camera was produced between 2008 and 2016 (serial numbers 000 to 011) and a high-definition (HD) version with a 4 Megapixel greyscale camera was produced between 2016 and 2021 (serial numbers 200 to 223). The smaller and more versatile UVP6 (Picheral et al., 2022) is commercially available since 2019. In the standard setting, the UVP5 images a volume of about 1 L at a frequency of 6 to 20 Hz and can be deployed down to 6000 m depth. Particles on each image are automatically sized. Further data processing of all particles allows calculations of the particle size distribution - the particle abundance or biovolume in increasing size intervals. The UVP5 STD version covers the size range from 102 μm to $\sim$ 50 mm ESD, the HD

version the size range from 64 μm to $\sim$ 50 mm ESD. Through reduction of the distance between the LED lights and the camera, the resolution can be further increased, but then the imaged volume is reduced. Inter-calibrated UVP5 units are globally in use by several teams. Since the UVP5 is mostly integrated in the CTD-Rosette and has its own pressure sensor, fine-scale vertical distribution of particles and major plankton groups can be related to environmental data obtained with other sensors mounted on the CTD-rosette. Most efforts regarding the analyses of UVP particle size spectra (including data from earlier versions such as the UVP4) have been on the estimation of particle biomass and flux by comparing them with particulate organic carbon (POC) collected in sediment traps or Niskin bottles (e.g., (Guidi et al., 2008b, 2015; Kiko et al., 2017; Stemmann et al., 2002, 2008a)). Particle abundance data was also used to estimate aerobic (Kalvelage et al., 2015; Thomsen et al., 2019) and anaerobic respiration (Bianchi et al., 2018; Karthäuser et al., 2021), to inform model development (Bianchi et al., 2018; Stemmann et al., 2004; Jouandet et al., 2014) or calibrate biogeochemical models (Niemeyer, 2020). Changes in the particle distribution were related to physical processes such as transport along continental margins (Stemmann et al., 2008b; Forest et al., 2013; de Madron et al., 1999), deep resuspension (Puig et al., 2013; de Madron et al., 2017) and mesoscale processes (Waite et al., 2016; Fiedler et al., 2016; Stemmann et al., 2008b; Guidi et al., 2012). Profound changes in bacterial activity at Oxygen minimum zone boundaries (Roullier et al., 2014) were related to enhanced particle abundance. Likewise, the importance of phyto- (Stemmann et al., 2002; Guidi et al., 2009) and zooplankton (Hauss et al., 2016; Christiansen et al., 2018; Stemmann et al., 2004) interactions with particles were assessed and the introduction of particles at depth via zooplankton Diel Vertical Migration reported (Kiko et al., 2017, 2020; Stemmann et al., 2000). In recent years, image analysis of large objects was performed and plankton organisms were discriminated from the detrital and abiotic particles in subsets of the dataset presented here, allowing the study of large plankton communities (Forest et al., 2012), bio-geography of specific taxa (Christiansen et al., 2018; Biard et al., 2016), zooplankton functional traits (Vilgrain et al., 2021) and particle types (Trudnowska et al., 2021).

1.4 The global marine particle size distribution dataset

Here we provide a dataset that was obtained with several inter-calibrated UVP5 units operated by different laboratories and during different cruises and projects around the world (Table 1). This international, collaborative effort resulted in a consistent, inter-calibrated global marine particle size distribution database that contains 8805 particle abundance and biovolume profiles obtained in all major oceans and several marginal seas since 2008. We provide further details about the UVP5, the inter-calibration and quality control procedures and the dataset structure in the Material and Methods section. Summarizing statistics, maps on data distribution, a description of global particle distribution and recommendations for use and further growth of the dataset are provided in the Results and Discussion sections.

2 Material and Methods

2.1 UVP5 description

The UVP5 consists of one downward-facing camera in a titanium pressure case and two sets of red LED lights that illuminate a 0.88 to 1.16 L-water volume (Picheral et al., 2010). The imaged volume depends on the actual instrument set-up which was determined experimentally for each set-up. During deployment - usually during the downcast of a CTD profile - the UVP5 takes 5-20 pictures of the illuminated volume of water per second. The particles in each image are counted and sized immediately and the data are stored in the instrument. Particle area is measured as the number of pixels (Sp) of an imaged object and can be converted to particle cross-sectional area (Sm) in mm^2 using: $Sm = Aa * Sp^{Exp}$. Here, Aa represents the area of one pixel in mm^2. Exp is a dimensionless adjustment factor. Aa and Exp need to be calibrated experimentally. To conduct the initial calibration for the dataset provided here, natural plankton and particle objects from the Bay of Villefranche-sur-Mer, France, were imaged in an aquarium with the UVP5 HD sn203 and using a stereo microscope during experiments conducted in fall 2016. Optimal values for the parameters Aa and Exp were obtained by minimizing ΔS, defined as

$$\Delta S = \sum_i (\log(Aa \cdot S_{i,p_u}^{Exp}) - \log(S_{i,m_\mu}))^2$$

where S_{i,p_u} is the surface area in pixels of object i as seen by the UVP and S_{i,m_μ} is the surface area in mm^2 of the same object i measured under the stereomicroscope. The minimization was performed using the Nelder-Mead simplex algorithm (implemented in the MATLAB function *fminsearch*). For this calibration experiment an Aa of 0.0036 mm^2 (interquartile range from -0.0002 to 0.0074 mm^2), an Exp of 1.149 (interquartile range 1.016 to 1.282) and an r^2 of 0.88 were found. Further details regarding the initial calibration procedure for the UVP5 SD version that was also applied to obtain the UVP5 HD calibration coefficients are given in Picheral et al. (2010).

2.2 Instrument inter-calibration

As several UVP5 units were produced, an inter-calibration procedure was developed to allow comparability of data from these units. The inter-calibration procedure is based on a comparison between one or several reference units (in particular sn002 and sn203) and the units to be calibrated. The imaged volume of each unit is determined, before the instruments are deployed at sea simultaneously on the same instrument carrier and the normalized size spectra are calculated. These operations have been performed since 2008 in the Mediterranean Sea off Nice, France. Figure 1a shows an example of raw data from a parallel deployment of a reference unit (sn002) and a unit under calibration (sn200). The Aa and Exp of the sn200 is then adjusted, so that after post-processing the normalized size spectra of both units coincide (Figure 1b). The reference units were regularly inter-calibrated against each other to check for possible drifts and improved data consistency. The development of the HD version of the UVP5 in 2016 required a revision of the UVP5 inter-calibration procedure, as pixel resolution has changed (Picheral et al., 2010). The calibration obtained for the HD unit sn203 in fall 2016 was propagated to several STD model reference units via simultaneous deployment at sea and subsequent calculation of correction factors. Thereafter, the corrections

obtained for the reference units were digitally propagated to all previously used UVP5 by reanalysing the earlier calibration experiment data. How the uncertainties of the initial calibration of the HD model sn203 propagate to the other UVP5 units and if these uncertainties can be reduced need to be further investigated.

2.3 Data collection, processing, quality control and dataset description

Metadata (position, time) of each profile collected in the presented dataset were checked by the respective data owners. All instrument settings and calibration coefficients for all cruises and projects were checked and, if necessary, corrected to match the HD inter-calibration results using automatic routines. Data from all cruises were then reprocessed using Zooprocess (https://sites.google.com/view/piqv/zooprocess) to obtain a coherent and inter-calibrated dataset, based on the HD inter-calibration conducted in fall 2016. For easier access and preliminary sharing, the data were then uploaded to EcoPart (http://ecopart.obs-vlfr.fr). To enable the archiving at Pangaea, data were directly downloaded from the EcoPart SQL database using a dedicated Python script and separated into three-year splits to obtain smaller file sizes and to enable the subsequent addition of further data.

During processing, the silhouette area of each particle is calculated as described above and then converted to an equivalent spherical diameter (ESD) according to $ESD = \sqrt{4 * Sm/\pi}$. Biovolume is calculated assuming a spherical particle using $Biovolume = ESD^3 * \pi/6$. Particles in a certain size class (e.g., ESD: 0.0403 - 0.0508 mm) and within a 5 dbar depth range are then counted and divided by the total observed volume to yield the particle abundance (#/L) in this size and depth interval. Likewise, the biovolume of individual particles is added up and divided by the observed volume to yield biovolume in mm^3/L. Size class bins are evenly spaced in a natural logarithmic scale, starting at 0.001 mm and ending at 26 mm, with in total 45 size bins. Size class bin width is hence increasing with size in a logarithmic fashion. Due to the detection limits of the UVP5, size class bins smaller 0.0403 mm ESD are empty and not reported, the largest size bin covers the size range from 20.6 to 26 mm ESD. Particle abundance and biovolume of particles with an ESD > 26 mm is also provided as an additional value. Data in this form is available on the EcoPart server. Quality-checked data was downloaded from the server on May 26, 2021 and submitted to Pangaea (https://doi.pangaea.de/10.1594/PANGAEA.924375). Apart from the particle abundance and biovolume in different size classes, the dataset contains the cruise id, the EcoPart Project identifier (integer), the Profile identifier, the filename of the raw file, the filename of an accompanying ctd profile (if this exists), latitude, longitude (both in decimals), date and time (in UTC), an EcoPart internal station identifier (integer), depth (indicated via the middle value of the 5 dbar depth bin; in dbar) and the observed volume per depth bin (in L). The particle size distribution data reported is inclusive of all living and non-living particles across the size range of detection. The dataset (available at https://doi.pangaea.de/10.1594/PANGAEA.9243751) contains all individual profile data. Also the values of AA, Exp, the imaged volume for each data acquisition, links to CTD data and other metadata are archived at Pangaea in the "Metadata collection for a global marine particle size distribution dataset obtained with the Underwater Vision Profiler 5", together with the dataset presented here.

Users of this dataset need to be aware that we provide the data as is, aggregated in 5 dbar depth bins. The particle size that can be quantified reliably with the UVP is limited at the lower end by the optical resolution of the camera and at the

upper end by the imaged volume. The optical resolution differs between the different UVP units used. In most cases, the lower size limit is at 0.102 mm (UVP5 SD) or 0.064 mm ESD (UVP5 HD), it is sometimes even lower, i.e., 0.203 or 0.256 mm ESD for early SD deployments. Also, several datasets exist that have a lower limit of 0.0403 mm ESD. In these cases the distance of the camera system to the illuminated field was reduced to increase image resolution. Projects with project ids 33 to 38 (uvp5_sn002zd_cascade2011, uvp5_sn002zd_ccelter_2011, uvp5_sn002zd_gatekeeper2010, uvp5_sn002zd_keops2, uvp5_sn002zd_keops2, uvp5_sn002zd_omer, uvp5_sn002zd_omer_2) and 50 to 51 (uvp5_sn003zp_pelgas2012, uvp5_sn003zp_tara2012) are concerned. In this case the imaged volume was reduced to 0.48 and 0.37 L, respectively. We would like to note that many UVP users do not use the first bin or even the first two or three bins of the size distribution of a given dataset in their analyses, as the particle size estimates at the lower resolution limit only rely on very few image pixels and therefore might be less reliable or noisy. The lower limit can be identified by computing a size spectrum with all depth bins of the profile or with the entire project dataset included. The bin where the differential particle size distribution peaks then represents the limit below which data should be considered as not quantitative. To yield better count statistics at the upper end of the size distribution, UVP users often also combine abundance or biovolume estimates from several depth bins. This is not only possible for the abundance estimates, but also for the biovolume estimates, as the reported biovolumes are the sum of the individual spherical volumes computed from each particle. The aggregation of depth bins leads to a loss of depth resolution, but increases the reliability of the count statistics, especially at the upper end of the size spectrum where particles are rare. To further define the upper limit of the size spectrum, one could also set the abundance and biovolume estimate to *nan* (not a number) if only one particle was observed in the aggregated volume. The count of particles per size bin can be computed by multiplying particle abundance and observed volume. Please also see Bisson et al. (2021) for a more in-depth analysis of the impact of count statistics on the estimation of particle abundance and particle flux. Their analysis shows that uncertainties of particle count statistics lead to an approximately 2-fold uncertainty of resulting particle flux estimates. Overall, we recommend careful consideration of the size range to be analysed for each individual cruise or project, as instruments used and their settings differ between each other, which can lead to different count statistics at the lower and upper ends of the size spectrum.

To enable visualization within this article, we aggregated particle abundance as in Kiko et al. (2017) into micrometric- (MiP: 0.14 to 0.53 mm ESD) and macroscopic particles (MaP: 0.53 mm to 16.88 mm ESD), and calculated the slope k of the differential particle size distribution as a descriptor of the relationship between particle abundance and size (Stemmann and Boss, 2012). This relationship is generally approximated by a two-parameter power-law function: $N = bd^{-k}$, where b and k are constants and d is the mean particle diameter for a given diameter range (dr). The differential particle abundance N can be calculated as the total number of objects per unit volume in the given diameter range dr (e.g. 0.203 mm to 0.256 mm) divided by the diameter range (in this case 0.053 mm) and is given as the number of particles per volume per size. To obtain an estimate of k, which is also referred to as the slope of the particle size distribution, one can then conduct a linear regression of $\log(N)$ vs. $\log(d)$ as $\log(N) = \log(b) - k(\log(d))$. The PSD slope k is calculated for the size range 0.203 mm to 2.05 mm, as this is the size range where the slope is mostly linear. These slope k is only considered if the p-value of the regression is < 0.05, otherwise the value is set to *nan* (not a number).

Already published datasets (Table 2) use different calibration coefficients which are not consistent with the HD inter-calibration procedure and differences may arise when comparing the different dataset versions. As an example we calculated abundances of two size classes and spectral slopes using the datasets from RV Maria S Merian cruise MSM23 and several RV Meteor cruises. MiP abundances are 4.2 (median; interquartile range 3.8 to 4.7) times larger with the new calibration factors, whereas MaP abundances are 1.5 times larger (median; interquartile range 1.2 to 2.0). Estimates of the slope k of the PSD are 1.09 (median; interquartile range 1.05 to 1.12) times larger. These factors were calculated using the datasets from RV Maria S Merian cruise MSM23 and RV Meteor cruises M92, M96 and M107 for which archived datasets with the relevant data exist. In our view, these changes are related to the increased resolution of the HD version (compared to the SD version) that enabled us to better quantify small particles during the initial laboratory calibration experiment for UVP5 HD sn203. This improved calibration was then propagated to all other units and superseded the earlier calibration experiment done with an SD unit.

We do not distinguish UVP5 particle data into distinct categories, such as copepods, aggregates, fecal pellets or other taxonomic or morphologic classes. For UVP5 data, this is possible for objects > 1 mm ESD, as the UVP5 also retrieves "vignettes" - small thumbnail images of respective regions of interest. Homogeneous identification of these vignettes among different cruises and operators is a time-consuming task and was not yet achieved for the entire dataset. Data from a subset of profiles are currently being prepared for publication.

3 Results and Discussion

3.1 Data distribution

The global distribution of UVP5 profiles contained in the published dataset is shown in Figure 2; in total, it comprises 8805 profiles, collected between 2008-06-19 and 2020-11-23 and between 81.3695 °N and 75.289 °S. The dataset represents a compilation of particle data from numerous small regional-scale research cruises as well as several large-scale hydrographic transects with bathypelagic and cross-basin coverage. All major ocean basins, the Mediterranean and the Baltic Sea were sampled. Most data is available from the Mediterranean Sea, the tropical Atlantic and Pacific, the Gulf of Alaska and the Arctic. Information on the number of profiles obtained per year, month and depth level is shown in Figure 3. The majority of profiles was collected in the upper 1000 m of the water column in June and August. Between 217 and 1146 profiles per year were obtained between 2008-2018. Almost all UVP5 data obtained between 2008 and 2019 are contained in our dataset. We were not able to obtain data from all UVP5 owners and can therefore not provide an exact estimate of how many profiles are currently missing from the dataset. Furthermore, some datasets obtained in 2019 and 2020 still require processing and will be added in subsequent updates of the dataset. Sampling effort is biased to the Northern hemisphere summer. Of all 8805 profiles, 1676 (19%) are shallower than 200 dbar, 7127 (80%) cover the upper 200 dbar of the water column, 3426 (38%) the upper 1000 dbar and 1018 (11%) go down to at least 3000 dbar. Deep profiles are mostly full depth profiles. The deepest profile reached 6017.5 dbar depth. Figure 4 shows the maximum depth per 2 degree grid box, whereas figure 5 shows the number of profiles obtained per 2 degree grid box.

3.2 Global particle abundance patterns

The global UVP5 particle dataset enables the characterisation of particle abundance and size structure patterns at a global scale, but also enables specific insights into particle dynamics at several regional study sites (e.g., the Gulf of Alaska, the California, Humboldt, Benguela and Mauretania upwelling systems and the Mediterranean Sea). Here, we aim to provide a short description of global particle distribution patterns and reference a few, already published studies. We use the terms micrometric particles (MiP) for particles with 0.14 to 0.53 mm ESD and macroscopic particles (MaP) for particles with 0.53 mm to 16.88 mm diameter) as in Kiko et al. (2017). Thereby, we also follow an approach used for marine aggregates, where those larger than 0.5 mm ESD are defined as marine snow (Suzuki and Kato, 1953; Alldredge and Silver, 1988). Globally, MiP and MaP concentrations in the upper 200 m are very variable (Figures 6, 9). High MiP and MaP particle abundance in coastal regions, in upwelling or frontal zones (MiP maximum values > 50000 #/L, MaP maximum values > 2000 #/L) are likely due to higher biological production and coastal inputs (Guidi et al., 2008a; Stemmann et al., 2008b; Roullier et al., 2014; Kiko et al., 2017). Particle concentrations are lower in oligotrophic gyres (MiP minimum values: 0.81 #/L MaP minimum values, 0.0 #/L MaP) where productivity and advective input from coastal regions are low (Guidi et al., 2008a, 2009; Stemmann et al., 2008a; Guidi et al., 2015). Particle abundance generally declines from the surface to depth (compare Figures 5, 6 and 7, as well as 8, 9 and 10). MiP and MaP in the meso- and bathy-pelagic layers also show a pattern consistent with the upper surface pattern probably as a consequence of passive flux of sinking particles (Guidi et al., 2015) and the active supply of particles via diel vertical migrations of zooplankton and nekton to the mesopelagic (Kiko et al., 2017, 2020). The strength of these supply mechanisms is dependent on the biological productivity at the surface, the strength of the active transport processes and the attenuation processes in the mesopelagic (Guidi et al., 2009). For the following analyses of vertical particle distribution in the open ocean, we only use data from profiles that were conducted down to at least 3000 dbar. For this subset, we find that MiP concentrations range from 0.81 to 53486.0 #/L between 0-200 dbar (median: 52.6, mean: 315.67, std: 1269.53), 1.29 to 38580.0 #/L between 200-1000 dbar (median: 21.76, mean: 54.39, std: 228.86) and 0.7 to 3184.0 #/L between 1000-3000 dbar (median: 12.6, mean: 15.47, std: 23.76). MaP concentrations ranging from 0.0 to 2130.1 #/L between 0-200 dbar (median: 0.75, mean: 6.17, std: 47.52), 0.0 to 2560.0 #/L between 200-1000 dbar (median: 0.15, mean: 0.89, std: 5.17) and 0.0 to 77.77 #/L between 1000-3000 dbar (median: 0.07, mean: 0.16, std: 0.57). The decline of particle abundance with depth has been interpreted as a consequence of microbial and metazoan flux attenuation (Stemmann et al., 2004; Guidi et al., 2009). The variability in MiP and MaP abundance range also decreases from the epi- to the bathy-pelagic, suggesting a feedback mechanism where high particle abundance results in strong flux attenuation by metazoans, thereby removing peaks in particle abundance and flux (Guidi et al., 2009).

3.3 Slope of the particle size distribution

The size distribution of particles is a basic property of marine systems, affecting trophic interactions, the vertical transmission of solar energy and the downward transport of organic matter Stemmann and Boss (2012). Despite its fundamental importance, size distribution is difficult to measure because particles occur over a large range of size and composition, from sub-micrometer

compact particles to large, cm-sized loose aggregates (Jackson et al., 1995; Stemmann et al., 2008a; Lombard et al., 2019). We here use the differential particle size distribution as e.g. described by Stemmann and Boss (2012). A slope k of 4 of the differential particle size distribution suggests an equal amount of mass in logarithmic increasing size intervals. By combining instruments over a μm to cm size range it was shown that the value of the slope varies greatly around the typical value of 4 (Jackson et al., 1995; Stemmann et al., 2008a). Our study also shows that the slope k varies greatly in the epi-, meso- and bathypelagic (Figures 12, 13 and 14). If we constrain the dataset to profiles that go deeper than 3000 dbar, the global mean value of the slope k in the top 200 dbar of the water column is found to be -3.57 +/- 0.56 std (minimum -6.58, maximum -1.8), with significant variations from -4 which are likely due to local ecosystem processes and other impacts. The average slope k and the variability remain similar at greater depth (-3.59 +/- 0.67 std, minimum -8.25, maximum -1.37 at 200-1000 dbar depth, -3.52 +/- 0.6 std, minimum -7.34, maximum -1.33 at 1000 to 3000 dbar depth). Throughout all depth ranges, steepest slopes are observed in oligotrophic basins such as the Eastern Mediterranean Sea and the center of the South Pacific gyre, while flatter spectra are observed in more productive regions such as the Western Mediterranean Sea and at high latitudes. These observations confirm earlier work using more restricted datasets (Guidi et al., 2009; Stemmann et al., 2008c; Guidi et al., 2008a). Earlier work based on a sub-sample of the dataset has also shown that the slope of the size spectrum is correlated with the phytoplankton community composition (Guidi et al., 2009; Stemmann et al., 2002) and can show diel variability related to zooplankton migration (Stemmann et al., 2000). Deeper in the water column, the spatial pattern of the slope k mostly reflects the upper ocean variability. Interestingly, bathypelagic values of k in the Antarctic are relatively flat, compared to temperate and tropical regions, which suggests that, in the Antarctic deep sea the relative role of larger, aggregated particles is more important than in the temperate and tropical regions. Such trend is not observed in data from Arctic regions.

3.4 Potential uses of the data

A further, detailed analysis of the provided dataset is beyond the scope of this article. Observation of a particle at a certain depth always generates the question how it was formed or arrived at the given location. Many attempts have been carried out to relate the UVP particle size spectrum with flux measured in sediment traps or by Thorium (Guidi et al., 2008b; Forest et al., 2013; Guidi et al., 2015), sinking speed (Stemmann et al., 2002) and POC (Stemmann et al., 2008a) but deriving biogeochemical properties from particle size is certainly an area for future progress. In these regards, our dataset should enable further regional and global analyses of particle dynamics (see e.g. Bisson et al. (2021)) and - in combination with flux estimates from sediment traps and/or Thorium isotope measurements, but also environmental data from satellites and other sources - enable us to better constrain the particle flux component of the biological pump (see e.g. Clements et al. (2021a, b)). However, we would like to stress that although the particles in our dataset are not per se sinking (e.g., also living zooplankton are treated as particles), particle abundance and size alone are still important information. Therefore, the data is also especially useful to constrain models that explicitly generate a particle size spectrum (Bianchi et al., 2018; Niemeyer, 2020; Weber and Bianchi, 2020; Stemmann et al., 2004; Jouandet et al., 2014). On the other hand particle data can also be used to estimate remineralization rates (Kalvelage et al., 2015; Bianchi et al., 2018; Thomsen et al., 2019; Karthäuser et al., 2021) or study trace element scavenging.

3.5 Recommendations for further instrument usage and growth of the dataset

This work presents the first attempt to establish a calibrated global data set of UVP measurements. Our analysis led us to develop a set of recommendations for future expansion of the global UVP data set. First of all, we recommend that full depth profiles are always taken at locations shallower than 1000 m depth and that otherwise at least the full mesopelagic down to 1000 m depth be sampled when using the UVP5. This is motivated by the fact that particle processes (indicated via a large range of e.g., MiP and MaP abundance) at these depths are very dynamic and require high resolution sampling. Below 1000 m depth, particle spatial patterns are less variable. Nevertheless, if sampling during a research cruise is conducted at water depths > 1000 m, full depth profiles or profiles down to the maximum depth rating of the used instruments (typically 6000m) should be done as often as possible. The deep sea is not well characterized with respect to abundance and size of particles and these comparatively small demands on shiptime will generate an important added value, as this will e.g. enable us to further assess carbon sequestration in the deep sea. It needs to be reiterated that a larger sampling volume will improve count statistics, especially for larger, rarer particles (Bisson et al., 2021). It should therefore be considered in sampling programs to conduct repeated profiles at a station to increase the effective sampled volume for a given station. Regions that are not well sampled until now are the Indian Ocean, Antarctic waters and the Western Pacific. Furthermore, winter data from both hemispheres is mostly lacking as well. In general, the UVP should be used during repeat hydrography programs as the operational goals of these programs to cover a representative fraction of the ocean (global and full depth coverage) align with our goals to create a global particle size distribution dataset. SCOR working group 154 "Integration of Plankton-Observing Sensor Systems to Existing Global Sampling Programs (P-OBS)" recommended the use of the UVP during the GO-ship program and similar sea-going expeditions (Boss et al., 2020). Data from the smaller and more versatile UVP6 (Picheral et al., 2022) that can also be deployed on gliders, floats, moorings and other vectors should also be integrated in future datasets and will enable the study of particle dynamics at spatial and temporal scales that are not accessible with the UVP5. Ancillary data that is useful for the interpretation of UVP data are temperature, salinity, oxygen and nutrient measurements, measurements of current dynamics, but also any measurements of particle dynamics and characteristics (e.g., Thorium-isotope measurements, lipid-content, elemental composition, particle sinking speed, sedimentation flux) and data on bacterio- phyto- and zooplankton composition. The latter are especially needed to understand the ecological processes behind the observed size spectra of particles and their subsequent export. The evaluation of the relative proportions of living and non-living particles is particularly important at the large size range (few hundreds of micrometer) because large, possibly sinking particles may be confused with zooplankton and lead to overestimation of particle stock and flux (Kiko et al., 2020). In the future, better automatic image classification algorithms may help to discriminate between non-living particles and plankton organisms and even provide information on other properties than their size (Stemmann and Boss, 2012; Trudnowska et al., 2021). We strongly recommend that regular inter-calibration experiments of all instruments against one or several standard units take place to maintain the data quality of all UVP units at an inter-operable level.

4 Conclusions

Here we provide the first global particle size spectra dataset containing 8805 profiles that were obtained with the UVP5 between 2008 and 2020. All UVP5s used were inter-calibrated with a standard procedure, calibration coefficients and metadata were checked and all profile data were reprocessed. This dataset therefore is internally consistent and supersedes earlier versions of cruise-specific UVP5 particle size spectrum data. The analysis of this global dataset shows that particle abundances are high in regions of high primary productivity and in coastal areas. Further analysis of the dataset should enable insights on different aspects of particle dynamics such as the effects of mesoscale features and Oxygen Minimum Zones, the fate of particulate matter in the deep sea and many other important aspects of the oceans biogeochemistry.

5 Data availability

The global UVP5 particle dataset Kiko et al. (2021) is publicly available at https://doi.pangaea.de/10.1594/PANGAEA.924375. The dataset was downloaded from the https://ecopart.obs-vlfr.fr/ server on the 15.February 2022.

Author contributions.

RK, MP and LS formulated the goals for data aggregation, quality control and the publication of a global UVP5 dataset. RK and MP led the quality control endeavors, supported by all co-authors. RK and LS conceived and drafted the article. All authors participated writing the article.

Competing interests.

The authors declare no competing interest.

Acknowledgements. RK acknowledges support via a "Make Our Planet Great Again" grant of the French National Research Agency within the "Programme d'Investissements d'Avenir"; reference "ANR-19-MPGA-0012" and via EU H2020 grant (agreement 817578 TRIATLAS project). RK and HH furthermore acknowledge support by the DFG-funded collaborative research center 754 "Climate-biogeochemistry interactions in the tropical Ocean" (Work Package B8) and the "CUSCO—Coastal Upwelling System in a Changing Ocean" project (Grant no. 03F0813A; Work package 5) funded by the Federal Ministry of Education and Research (Germany). The McDonnell Laboratory at the University of Alaska Fairbanks acknowledges support from the U.S. National Science Foundation (Award numbers 1654663 and 1656070), the U.S. National Aeronautics and Space Administration (Award number 80NSSC17K0692), and the M.J. Murdock Charitable Trust. The collection of data by the University of Maine were funded by NASA grants NNX15AE67G (NAAMES) and 80NSSC17K0568 (EXPORTS). We thank the support of CNRS-INSU through the MISTRALS-MERMEX program. LS was supported by the Chair Vision between CNRS

and Sorbonne University. We would like to thank Hela Mehrtens (GEOMAR Helmholtz Center for Ocean Kiel, Germany) for her help with the submission to the PANGAEA data archive.

References

Alldredge, A. L. and Gotschalk, C.: In situ settling behavior of marine snow 1, Limnology and Oceanography, 33, 339–351, 1988.

Alldredge, A. L. and Silver, M. W.: Characteristics, dynamics and significance of marine snow, Progress in oceanography, 20, 41–82, 1988.

Asper, V. L.: Measuring the flux and sinking speed of marine snow aggregates, Deep Sea Research Part A. Oceanographic Research Papers, 34, 1–17, 1987.

Beebe, W.: A Round Trip to Davy Jone's Locker, National Geographic Magazine, LIX, 1931.

Benfield, M. C., Grosjean, P., Culverhouse, P. F., Irigoien, X., Sieracki, M. E., Lopez-Urrutia, A., Dam, H. G., Hu, Q., Davis, C. S., Hansen, A., et al.: RAPID: research on automated plankton identification, Oceanography, 20, 172–187, 2007.

Bianchi, D., Weber, T. S., Kiko, R., and Deutsch, C.: Global Niche of Marine Anaerobic Metabolisms Expanded by Particle Microenvironments, Nature Geoscience, 11, 263–268, https://doi.org/10.1038/s41561-018-0081-0, 2018.

Biard, T., Stemmann, L., Picheral, M., Mayot, N., Vandromme, P., Hauss, H., Gorsky, G., Guidi, L., Kiko, R., and Not, F.: In situ imaging reveals the biomass of giant protists in the global ocean, Nature, 532, 504–507, 2016.

Bisson, K. M., Kiko, R., Siegel, D. A., Guidi, L., Picheral, M., Boss, E., and Cael, B. B.: Sampling uncertainties of particle size distributions and derived fluxes, https://doi.org/10.1002/essoar.10508460.1, https://doi.org/10.1002/essoar.10508460.1, 2021.

Boss, E., Waite, A. M., Uitz, J., Acinas, S. G., Sosik, H. M., Fennel, K., Berman-Frank, I., Cornejo, M., Thomalla, S., Yamazaki, H., Batten, S., Berg, J., Claustre, H., Grégori, G., Karstensen, J., Muller-Karger, F., Richardson, A., Sloyan, B., Wanninkhof, R., Ras, J., Dimier, C., Cetinić, I., Duforêt, L., Clemenston, L., Ferrera, I., Gasol, J. M., Massana, R., Sánchez, P., Sebastián, M., Sunagawa, S., Garczarek, L., de Vargas, C., Pesant, S., Mathew, S., Campbell, L., Brosnahan, M., Poulton, N., Marie, D., Gaube, P., Downie, R., Kloser, R., Lee, W.-J., Sato, M., Roesler, C., Dall'Olmo, G., Slade, W., Twardowski, M., Gardner, W., Briggs, N., Xing, X., Organelli, E., Frouin, R., Barone, B., McDonnel, A., Liu, Y., Chase, A., Miloslavich, P., Lombard, F., Behrenfeld, M., Jumars, P., and Karp-Boss, L.: Recommendations for plankton measurements on the GO-SHIP program with relevance to other sea-going expeditions, SCOR Working Group 154 GO-SHIP Report, 2020.

Boyd, P. W., Claustre, H., Levy, M., Siegel, D. A., and Weber, T.: Multi-Faceted Particle Pumps Drive Carbon Sequestration in the Ocean, 568, 327–335, https://doi.org/10.1038/s41586-019-1098-2, https://www.nature.com/articles/s41586-019-1098-2.

Checkley Jr, D., Davis, R., Herman, A., Jackson, G., Beanlands, B., and Regier, L.: Assessing plankton and other particles in situ with the SOLOPC, Limnology and Oceanography, 53, 2123–2136, 2008.

Christiansen, S., Hoving, H.-J., Schütte, F., Hauss, H., Karstensen, J., Körtzinger, A., Schröder, S.-M., Stemmann, L., Christiansen, B., Picheral, M., et al.: Particulate matter flux interception in oceanic mesoscale eddies by the polychaete Poeobius sp., Limnology and Oceanography, 63, 2093–2109, 2018.

Clements, D. J., Yang, S., Weber, T., McDonnell, A., Kiko, R., Stemmann, L., and Bianchi, D.: Constraining the Ocean's Biological Pump with in Situ Optical Observations and Supervised Learning. Part 2: Carbon Flux | Earth and Space Science Open Archive, https://www.essoar.org/doi/10.1002/essoar.10509084.3, 2021a.

Clements, D. J., Yang, S., Weber, T., McDonnell, A., Kiko, R., Stemmann, L., and Bianchi, D.: Constraining the Ocean's Biological Pump with in Situ Optical Observations and Supervised Learning. Part 1:Particle Size Distributions, https://doi.org/10.1002/essoar.10509083.1, http://www.essoar.org/doi/10.1002/essoar.10509083.1, 2021b.

Cózar, A., Echevarría, F., González-Gordillo, J. I., Irigoien, X., Úbeda, B., Hernández-León, S., Palma, Á. T., Navarro, S., García-de Lomas, J., Ruiz, A., et al.: Plastic debris in the open ocean, Proceedings of the National Academy of Sciences, 111, 10 239–10 244, 2014.

de Madron, X. D., Radakovitch, O., Heussner, S., Loye-Pilot, M., and Monaco, A.: Role of the climatological and current variability on shelf-slope exchanges of particulate matter: Evidence from the Rhône continental margin (NW Mediterranean), Deep Sea Research Part I: Oceanographic Research Papers, 46, 1513–1538, 1999.

de Madron, X. D., Ramondenc, S., Berline, L., Houpert, L., Bosse, A., Martini, S., Guidi, L., Conan, P., Curtil, C., Delsaut, N., et al.: Deep sediment resuspension and thick nepheloid layer generation by open-ocean convection, Journal of Geophysical Research: Oceans, 122, 2291–2318, 2017.

Duarte, C. M., Marbà, N., Gacia, E., Fourqurean, J. W., Beggins, J., Barrón, C., and Apostolaki, E. T.: Seagrass Community Metabolism: Assessing the Carbon Sink Capacity of Seagrass Meadows, Global Biogeochemical Cycles, 24, https://doi.org/10.1029/2010GB003793, 2010.

Fiedler, B., Grundle, D., Schütte, F., Karstensen, J., Löscher, C., Hauss, H., Wagner, H., Loginova, A. N., Kiko, R., Silva, P., et al.: Oxygen utilization and downward carbon flux in an oxygen-depleted eddy in the eastern tropical North Atlantic, Biogeosciences (BG), 13, 5633–5647, 2016.

Forest, A., Stemmann, L., Picheral, M., Burdorf, L., Robert, D., Fortier, L., and Babin, M.: Size distribution of particles and zooplankton across the shelf-basin system in southeast Beaufort Sea: combined results from an Underwater Vision Profiler and vertical net tows, Biogeosciences, 9, 1301, 2012.

Forest, A., Babin, M., Stemmann, L., Picheral, M., Sampei, M., Fortier, L., Gratton, Y., Bélanger, S. D., Sahlin, J., Doxaran, D., et al.: Ecosystem function and particle flux dynamics across the Mackenzie Shelf (Beaufort Sea, Arctic Ocean): an integrative analysis of spatial variability and biophysical forcings., Biogeosciences, 10, 2833–2866, 2013.

German, C. and Von Damm, K.: Hydrothermal processes, Treatise on geochemistry, 6, 625, 2003.

Giering, S. L. C., Cavan, E. L., Basedow, S. L., Briggs, N., Burd, A. B., Darroch, L. J., Guidi, L., Irisson, J.-O., Iversen, M. H., Kiko, R., Lindsay, D., Marcolin, C. R., McDonnell, A. M. P., Möller, K. O., Passow, U., Thomalla, S., Trull, T. W., and Waite, A. M.: Sinking Organic Particles in the Ocean—Flux Estimates From in situ Optical Devices, Frontiers in Marine Science, 6, 834, https://doi.org/10.3389/fmars.2019.00834, https://www.frontiersin.org/article/10.3389/fmars.2019.00834, 2020.

Gorsky, G., Picheral, M., and Stemmann, L.: Use of the Underwater Video Profiler for the study of aggregate dynamics in the North Mediterranean, Estuarine, Coastal and Shelf Science, 50, 121–128, 2000.

Gorsky, G., Prieur, L., Taupier-Letage, I., Stemmann, L., and Picheral, M.: Large particulate matter in the Western Mediterranean: I. LPM distribution related to mesoscale hydrodynamics, Journal of Marine Systems, 33, 289–311, 2002.

Guidi, L., Gorsky, G., Claustre, H., Miquel, J., Picheral, M., and Stemmann, L.: Distribution and fluxes of aggregates> 100 μm in the upper kilometer of the South-Eastern Pacific, 1foldr Import 2019-10-08 Batch 12, 2008a.

Guidi, L., Jackson, G. A., Stemmann, L., Miquel, J. C., Picheral, M., and Gorsky, G.: Relationship between particle size distribution and flux in the mesopelagic zone, Deep Sea Research Part I: Oceanographic Research Papers, 55, 1364–1374, https://doi.org/10.1016/j.dsr.2008.05.014, http://www.sciencedirect.com/science/article/pii/S0967063708001209, 2008b.

Guidi, L., Stemmann, L., Jackson, G. A., Ibanez, F., Claustre, H., Legendre, L., Picheral, M., and Gorskya, G.: Effects of phytoplankton community on production, size, and export of large aggregates: A world-ocean analysis, Limnology and Oceanography, 54, 1951–1963, 2009.

Guidi, L., Calil, P. H., Duhamel, S., Björkman, K. M., Doney, S. C., Jackson, G. A., Li, B., Church, M. J., Tozzi, S., Kolber, Z. S., et al.: Does eddy-eddy interaction control surface phytoplankton distribution and carbon export in the North Pacific Subtropical Gyre?, Journal of Geophysical Research: Biogeosciences, 117, 2012.

Guidi, L., Legendre, L., Reygondeau, G., Uitz, J., Stemmann, L., and Henson, S. A.: A new look at ocean carbon remineralization for estimating deepwater sequestration, Global Biogeochemical Cycles, 29, 1044–1059, https://doi.org/10.1002/2014GB005063, https://agupubs.onlinelibrary.wiley.com/doi/abs/10.1002/2014GB005063, 2015.

Hauss, H., Christiansen, S., Schütte, F., Kiko, R., Lima, M. E., Rodrigues, E., Karstensen, J., Löscher, C. R., Körtzinger, A., and Fiedler, B.: Dead zone or oasis in the open ocean? Zooplankton distribution and migration in low-oxygen modewater eddies, Biogeosciences, 13, 1977–1989, https://doi.org/10.5194/bg-13-1977-2016, 2016.

Herman, A. W.: Design and calibration of a new optical plankton counter capable of sizing small zooplankton, Deep Sea Research Part A. Oceanographic Research Papers, 39, 395–415, 1992.

Honjo, S., Doherty, K. W., Agrawal, Y. C., and Asper, V. L.: Direct optical assessment of large amorphous aggregates (marine snow) in the deep ocean, Deep Sea Research Part A. Oceanographic Research Papers, 31, 67–76, 1984.

Jackson, G. A.: A model of the formation of marine algal flocs by physical coagulation processes, Deep Sea Research Part A. Oceanographic Research Papers, 37, 1197–1211, 1990.

Jackson, G. A., Logan, B. E., Alldredge, A. L., and Dam, H. G.: Combining particle size spectra from a mesocosm experiment measured using photographic and aperture impedance (Coulter and Elzone) techniques, Deep Sea Research Part II: Topical Studies in Oceanography, 42, 139–157, 1995.

Jouandet, M.-P., Jackson, G. A., Carlotti, F., Picheral, M., Stemmann, L., and Blain, S.: Rapid formation of large aggregates during the spring bloom of Kerguelen Island: observations and model comparisons, 1foldr Import 2019-10-08 Batch 11, 2014.

Kalvelage, T., Lavik, G., Jensen, M. M., Revsbech, N. P., Löscher, C., Schunck, H., Desai, D. K., Hauss, H., Kiko, R., Holtappels, M., LaRoche, J., Schmitz, R. A., Graco, M. I., and Kuypers, M. M. M.: Aerobic Microbial Respiration In Oceanic Oxygen Minimum Zones, PLoS ONE, 10, e0133 526, https://doi.org/10.1371/journal.pone.0133526, http://dx.doi.org/10.1371%2Fjournal.pone.0133526, 2015.

Karthäuser, C., Ahmerkamp, S., Marchant, H. K., Bristow, L. A., Hauss, H., Iversen, M. H., Kiko, R., Maerz, J., Lavik, G., and Kuypers, M. M. M.: Small Sinking Particles Control Anammox Rates in the Peruvian Oxygen Minimum Zone, 12, 3235, https://doi.org/10.1038/s41467-021-23340-4, https://www.nature.com/articles/s41467-021-23340-4, 2021.

Katz, J., Donaghay, P., Zhang, J., King, S., and Russell, K.: Submersible holocamera for detection of particle characteristics and motions in the ocean, Deep Sea Research Part I: Oceanographic Research Papers, 46, 1455–1481, 1999.

Kiko, R., Biastoch, A., Brandt, P., Cravatte, S., Hauss, H., Hummels, R., Kriest, I., Marin, F., McDonnell, A., Oschlies, A., et al.: Biological and physical influences on marine snowfall at the equator, Nature Geoscience, 10, 852–858, 2017.

Kiko, R., Brandt, P., Christiansen, S., Faustmann, J., Kriest, I., Rodrigues, E., Schütte, F., and Hauss, H.: Zooplankton-Mediated Fluxes in the Eastern Tropical North Atlantic, Frontiers in Marine Science, 7, Art–Nr, 2020.

Kiko, R., Picheral, M., Antoine, D., Babin, M., Berline, L., Biard, T., Boss, E., Brandt, P., Carlotti, F., Christiansen, S., Coppola, L., de la Cruz, L., Diamond-Riquier, E., de Madron, X. D., Elineau, A., Gorsky, G., Guidi, L., Hauss, H., Irisson, J.-O., Karp-Boss, L., Karstensen, J., gyun Kim, D., Lekanoff, R. M., Lombard, F., Lopes, R. M., Marec, C., McDonnell, A., Niemeyer, D., Noyon, M., O'Daly, S., Ohman, M., Pretty, J. L., Rogge, A., Searson, S., Shibata, M., Tanaka, Y., Tanhua, T., Taucher, J., Trudnowska, E., Turner, J. S., Waite, A. M., and Stemmann, L.: The global marine particle size distribution dataset obtained with the Underwater Vision Profiler 5 - version 1, https://doi.pangaea.de/10.1594/PANGAEA.924375, 2021.

Lampitt, R., Hillier, W., and Challenor, P.: Seasonal and diel variation in the open ocean concentration of marine snow aggregates, Nature, 362, 737–739, 1993.

Lombard, F., Boss, E., Waite, A. M., Vogt, M., Uitz, J., Stemmann, L., Sosik, H. M., Schulz, J., Romagnan, J.-B., Picheral, M., Pearlman, J., Ohman, M. D., Niehoff, B., Möller, K. O., Miloslavich, P., Lara-Lpez, A., Kudela, R., Lopes, R. M., Kiko, R., Karp-Boss, L., Jaffe, J. S., Iversen, M. H., Irisson, J.-O., Fennel, K., Hauss, H., Guidi, L., Gorsky, G., Giering, S. L. C., Gaube, P., Gallager, S., Dubelaar, G., Cowen, R. K., Carlotti, F., Briseño-Avena, C., Berline, L., Benoit-Bird, K., Bax, N., Batten, S., Ayata, S. D., Artigas, L. F., and Appeltans, W.: Globally Consistent Quantitative Observations of Planktonic Ecosystems, Frontiers in Marine Science, 6, https://doi.org/10.3389/fmars.2019.00196, https://www.frontiersin.org/articles/10.3389/fmars.2019.00196/full, 2019.

Ludwig, W. and Probst, J.-L.: River sediment discharge to the oceans; present-day controls and global budgets, American Journal of Science, 298, 265–295, 1998.

Many, G., de Madron, X. D., Verney, R., Bourrin, F., Renosh, P., Jourdin, F., and Gangloff, A.: Geometry, fractal dimension and settling velocity of flocs during flooding conditions in the Rhône ROFI, Estuarine, Coastal and Shelf Science, 219, 1–13, 2019.

McCave, I.: Local and global aspects of the bottom nepheloid layers in the world ocean, Netherlands Journal of Sea Research, 20, 167–181, 1986.

McCave, I. N.: Nepheloid layers, Elements of physical oceanography: A derivative of the encyclopedia of ocean sciences, pp. 0–282, 2009.

Neal, E. G., Hood, E., and Smikrud, K.: Contribution of glacier runoff to freshwater discharge into the Gulf of Alaska, Geophysical Research Letters, 37, 2010.

Niemeyer, D.: Modelling features of the biological pump and its impact on marine oxygen distribution, Ph.D. thesis, 2020.

O'Hern, T. J., d' Agostino, L., and Acosta, A. J.: Comparison of Holographic and Coulter Counter Measurements of Cavitation Nuclei in the Ocean, 110, 200–207, https://doi.org/10.1115/1.3243535, https://doi.org/10.1115/1.3243535.

Picheral, M., Guidi, L., Stemmann, L., Karl, D. M., Iddaoud, G., and Gorsky, G.: The Underwater Vision Profiler 5: An advanced instrument for high spatial resolution studies of particle size spectra and zooplankton, Limnology and Oceanography: Methods, 8, 462–473, 2010.

Picheral, M. et al.: The Underwater Vision Profiler 6: an imaging sensor of particle size spectra and plankton, for autonomous and cabled platforms, Limnology and Oceanography: Methods, 2022.

Puig, P., de Madron, X. D., Salat, J., Schroeder, K., Martín, J., Karageorgis, A. P., Palanques, A., Roullier, F., Lopez-Jurado, J. L., Emelianov, M., et al.: Thick bottom nepheloid layers in the western Mediterranean generated by deep dense shelf water cascading, Progress in Oceanography, 111, 1–23, 2013.

Ratmeyer, V. and Wefer, G.: A high resolution camera system (ParCa) for imaging particles in the ocean: System design and results from profiles and a three-month deployment, Journal of Marine Research, 54, 589–603, 1996.

Ratmeyer, V., Fischer, G., and Wefer, G.: Lithogenic particle fluxes and grain size distributions in the deep ocean off northwest Africa: Implications for seasonal changes of aeolian dust input and downward transport, Deep Sea Research Part I: Oceanographic Research Papers, 46, 1289–1337, 1999.

Remsen, A., Hopkins, T. L., and Samson, S.: What You See Is Not What You Catch: A Comparison of Concurrently Collected Net, Optical Plankton Counter, and Shadowed Image Particle Profiling Evaluation Recorder Data from the Northeast Gulf of Mexico, 51, 129–151, https://doi.org/10.1016/j.dsr.2003.09.008, http://www.sciencedirect.com/science/article/pii/S0967063703001614, 2004.

Roullier, F., Berline, L., Guidi, L., Durrieu De Madron, X., Picheral, M., Sciandra, A., Pesant, S., and Stemmann, L.: Particle size distribution and estimated carbon flux across the Arabian Sea oxygen minimum zone, Biogeosciences, 11, 4541–4557, 2014.

Sheldon, R. and Parsons, T.: A practical manual on the use of the Coulter Counter in marine science, Coulter Electronics, Toronto, 66, 1967.

Stemmann, L. and Boss, E.: Plankton and particle size and packaging: from determining optical properties to driving the biological pump, Annual Review of Marine Science, 4, 263–290, 2012.

Stemmann, L., Picheral, M., and Gorsky, G.: Diel variation in the vertical distribution of particulate matter (> 0.15 mm) in the NW Mediterranean Sea investigated with the Underwater Video Profiler, Deep Sea Research Part I: Oceanographic Research Papers, 47, 505–531, 2000.

Stemmann, L., Gorsky, G., Marty, J.-C., Picheral, M., and Miquel, J.-C.: Four-year study of large-particle vertical distribution (0–1000 m) in the NW Mediterranean in relation to hydrology, phytoplankton, and vertical flux, Deep Sea Research Part II: Topical Studies in Oceanography, 49, 2143–2162, 2002.

Stemmann, L., Jackson, G. A., and Ianson, D.: A vertical model of particle size distributions and fluxes in the midwater column that includes biological and physical processes—Part I: model formulation, Deep Sea Research Part I: Oceanographic Research Papers, 51, 865–884, 2004.

Stemmann, L., Eloire, D., Sciandra, A., Jackson, G., Guidi, L., Picheral, M., and Gorsky, G.: Volume distribution for particles between 3.5 to 2000 μm in the upper 200 m region of the South Pacific Gyre, Biogeosciences, 5, 299–310, 2008a.

Stemmann, L., Prieur, L., Legendre, L., Taupier-Letage, I., Picheral, M., Guidi, L., and Gorsky, G.: Effects of frontal processes on marine aggregate dynamics and fluxes: An interannual study in a permanent geostrophic front (NW Mediterranean), Journal of Marine Systems, 70, 1–20, 2008b.

Stemmann, L., Youngbluth, M., Robert, K., Hosia, A., Picheral, M., Paterson, H., Ibanez, F., Guidi, L., Lombard, F., and Gorsky, G.: Global zoogeography of fragile macrozooplankton in the upper 100–1000 m inferred from the underwater video profiler, ICES Journal of Marine Science, 65, 433–442, 2008c.

Stemmann, L., Picheral, M., Guidi, L., Lombard, F., Prejger, F., Claustre, H., and Gorsky, G.: Assessing the spatial and temporal distributions of zooplankton and marine particles using the Underwater Vision Profiler, Sensors for ecology, p. 119, 2012.

Suzuki, N. and Kato, K.: Studies on suspended materials marine snow in the sea: Part . sources of marine snow, Bulletin of the Faculty of Fisheries of Hokkaido University, 4, 132–137, 1953.

Thomsen, S., Karstensen, J., Kiko, R., Krahmann, G., Dengler, M., and Engel, A.: Remote and local drivers of oxygen and nitrate variability in the shallow oxygen minimum zone off Mauritania in June 2014, Biogeosciences, 16, 979–998, 2019.

Trudnowska, E., Lacour, L., Ardyna, M., Rogge, A., Irisson, J. O., Waite, A. M., Babin, M., and Stemmann, L.: Marine Snow Morphology Illuminates the Evolution of Phytoplankton Blooms and Determines Their Subsequent Vertical Export, 12, 2816, https://doi.org/10.1038/s41467-021-22994-4, https://www.nature.com/articles/s41467-021-22994-4, 2021.

Vilgrain, L., Maps, F., Picheral, M., Babin, M., Aubry, C., Irisson, J.-O., and Ayata, S.-D.: Trait-Based Approach Using in Situ Copepod Images Reveals Contrasting Ecological Patterns across an Arctic Ice Melt Zone, 66, 1155–1167, https://doi.org/10.1002/lno.11672, https://aslopubs.onlinelibrary.wiley.com/doi/abs/10.1002/lno.11672, 2021.

Waite, A. M., Stemmann, L., Guidi, L., Calil, P. H., Hogg, A. M. C., Feng, M., Thompson, P. A., Picheral, M., and Gorsky, G.: The wineglass effect shapes particle export to the deep ocean in mesoscale eddies, Geophysical Research Letters, 43, 9791–9800, 2016.

Weber, T. and Bianchi, D.: Efficient Particle Transfer to Depth in Oxygen Minimum Zones of the Pacific and Indian Oceans, Frontiers in Earth Science, 8, https://doi.org/10.3389/feart.2020.00376, 2020.

Wiebe, P. H. and Benfield, M. C.: From the Hensen net toward four-dimensional biological oceanography, Progress in Oceanography, 56, 7–136, 2003.

Zhou, M.: What Determines the Slope of a Plankton Biomass Spectrum?, 28, 437–448, https://doi.org/10.1093/plankt/fbi119, https://doi.org/10.1093/plankt/fbi119.

Zuniga, D., Calafat, A., Heussner, S., Miserocchi, S., Sanchez-Vidal, A., Garcia-Orellana, J., Canals, M., Sánchez-Cabeza, J., Carbonne, J., Delsaut, N., et al.: Compositional and temporal evolution of particle fluxes in the open Algero–Balearic basin (Western Mediterranean), Journal of Marine Systems, 70, 196–214, 2008.

Tables

Table 1

Table 1: Geospatial information for UVP projects.

UVP project name	Ecopart ID	Profiles	Time period	Latitude range	Longitude range	UVP manager(s)
uvp5_sn000_boum2008	2	184	2008-06-19 to 2008-07-18	43.21 to 33.47	32.77 to 4.93	L Stemmann, M Picheral
uvp5_sn000_ccelter_2012	3	62	2012-07-28 to 2012-08-21	34.6 to 33.1	-118.31 to -123.69	L Stemmann, M Picheral
uvp5_sn000_lohafex2009	4	57	2009-01-16 to 2009-03-06	-47.58 to -50.01	-13.64 to -35.26	L Stemmann, M Picheral
uvp5_sn000_lter2008	5	75	2008-09-30 to 2008-10-28	34.2 to 32.15	-117.96 to -124.0	L Stemmann, M Picheral
uvp5_sn000_malina2009	16	154	2009-07-18 to 2009-08-22	72.06 to 69.47	-126.48 to -140.81	L Stemmann, M Picheral
uvp5_sn000_msm049	19	22	2015-11-30 to 2015-12-19	20.32 to 12.0	-20.5 to -24.28	R Kiko, H Hauss
uvp5_sn000_operex2008	20	92	2008-07-31 to 2008-08-12	25.75 to 22.24	-156.25 to -160.67	L Guidi, L Stemmann
uvp5_sn000_tara2009	6	46	2009-10-11 to 2009-12-15	43.36 to 33.37	35.33 to 7.89	L Stemmann, M Picheral
uvp5_sn000_tara2010	7	196	2010-01-09 to 2010-12-17	27.16 to -55.1	73.91 to -65.91	L Stemmann, M Picheral
uvp5_sn000_tara2011	99	264	2011-01-03 to 2011-12-21	35.42 to -64.36	-53.01 to -159.06	L Stemmann, M Picheral
uvp5_sn000_tara2012	9	32	2012-01-28 to 2012-02-18	39.24 to 32.92	-66.54 to -75.07	L Stemmann, M Picheral
uvp5_sn001_2012_moose_ge	21	87	2012-07-24 to 2012-08-08	43.9 to 40.0	9.64 to 3.44	L Stemmann, M Picheral
uvp5_sn001_2012_msm22	22	113	2012-10-24 to 2012-11-22	18.5 to -5.01	-19.68 to -26.99	R Kiko, H Hauss
uvp5_sn001_2012_msm23	23	64	2012-11-26 to 2012-12-16	17.6 to -18.19	1.0 to -24.3	R Kiko, H Hauss
uvp5_sn001_2013_m92	24	30	2013-01-19 to 2013-01-30	-11.0 to -12.61	-77.17 to -78.63	R Kiko, H Hauss
uvp5_sn001_2013_m93	25	148	2013-02-08 to 2013-03-04	-12.16 to -13.97	-76.42 to -78.42	R Kiko, H Hauss
uvp5_sn001_2013_m96	26	77	2013-05-02 to 2013-05-22	17.7 to 11.33	-20.08 to -60.3	R Kiko, H Hauss
uvp5_sn001_2013_m97	27	180	2013-05-26 to 2013-06-23	17.57 to 8.0	-17.75 to -24.28	R Kiko, H Hauss
uvp5_sn001_2013_m98	28	52	2013-07-02 to 2013-07-23	-5.12 to -11.5	13.5 to -35.89	R Kiko, H Hauss
uvp5_sn001_2014_msm40	29	5	2014-08-17 to 2014-08-19	59.54 to 59.19	-39.74 to -43.54	R Kiko, H Hauss
uvp5_sn002_iado_2014	251	26	2014-09-20 to 2014-09-23	43.69 to 43.37	7.89 to 7.14	J-O Irisson
uvp5_sn002_iado_2015	252	36	2015-09-16 to 2015-09-20	43.65 to 43.42	7.8 to 7.13	J-O Irisson
uvp5_sn002_iado_2016	30	16	2016-09-18 to 2016-09-21	43.67 to 43.39	7.6 to 7.31	J-O Irisson
uvp5_sn002_iado_2018	121	10	2018-09-22 to 2018-09-23	43.59 to 43.31	7.68 to 7.39	J-O Irisson
uvp5_sn002_moose_dyf_2013	10	4	2013-09-14 to 2013-10-24	43.42 to 43.42	7.9 to 7.9	L Stemmann, M Picheral
uvp5_sn002_moose_dyf_2014	11	9	2014-03-11 to 2014-12-10	43.68 to 43.36	7.9 to 7.31	L Stemmann, M Picheral
uvp5_sn002_moose_dyf_2015	12	9	2015-02-08 to 2015-12-10	43.44 to 43.42	7.87 to 7.82	L Stemmann, M Picheral
uvp5_sn002_moose_dyf_2016	13	10	2016-02-05 to 2016-12-10	43.43 to 43.41	7.87 to 7.86	L Guidi
uvp5_sn002_moose_dyf_2017	14	8	2017-02-07 to 2017-11-08	43.43 to 43.41	7.88 to 7.86	L Coppola
uvp5_sn002_moose_dyf_2018	166	4	2018-01-23 to 2018-08-27	43.42 to 43.41	7.87 to 7.85	L Guidi
uvp5_sn002_moose_ge_2013	15	6	2013-06-11 to 2013-06-15	43.75 to 43.41	9.36 to 7.52	L Stemmann, M Picheral

uvp5_sn002_moose_ge_2014	17	84	2014-07-04 to 2014-07-20	43.93 to 40.0	9.72 to 3.5	L Stemmann, M Picheral
uvp5_sn002_moose_ge_2015_filtered	31	72	2015-07-10 to 2015-07-27	43.88 to 40.0	9.63 to 3.54	L Stemmann, M Picheral
uvp5_sn002_moose_ge_2016_filtered	18	84	2016-05-19 to 2016-06-09	43.63 to 40.0	8.92 to 3.54	L Guidi
uvp5_sn002_moose_ge_2017_filtered	100	116	2017-08-31 to 2017-09-23	43.88 to 39.99	9.63 to 3.5	L Coppola
uvp5_sn002_moose_ge_2019	149	88	2019-06-08 to 2019-07-01	43.88 to 40.0	9.63 to 3.5	L Coppola
uvp5_sn002_somba_ge_2014	32	65	2014-08-17 to 2014-09-08	39.72 to 36.55	9.48 to -0.7	L Stemmann, M Picheral
uvp5_sn002zd_cascade2011	33	82	2011-03-02 to 2011-03-21	43.4 to 41.13	6.13 to 3.36	X. Durrieu de Madron
uvp5_sn002zd_ccelter_2011	34	58	2011-06-27 to 2011-07-16	34.11 to 32.58	-120.85 to -121.78	L Stemmann, M Picheral
uvp5_sn002zd_gatekeeper2010	35	21	2010-07-11 to 2010-07-14	36.8 to 36.7	-121.97 to -122.58	L Stemmann, M Picheral
uvp5_sn002zd_keops2	36	106	2011-10-14 to 2011-11-20	-45.0 to -50.65	75.0 to 52.1	L Stemmann, M Picheral
uvp5_sn002zd_keops2	36	106	2011-10-14 to 2011-11-20	-45.0 to -50.65	75.0 to 52.1	L Stemmann, M Picheral
uvp5_sn002zd_omer	37	10	2012-04-08 to 2012-04-09	43.61 to 43.58	7.58 to 7.49	L Stemmann, M Picheral
uvp5_sn002zd_omer_2	38	7	2012-05-20 to 2012-05-22	43.69 to 43.69	7.32 to 7.31	L Stemmann, M Picheral
uvp5_sn003_2015_kaxis	40	3	2016-01-21 to 2016-01-23	-61.97 to -62.7	95.37 to 91.53	L Stemmann, M Picheral
uvp5_sn003_cassiopee_2015	41	82	2015-07-20 to 2015-08-15	2.0 to -19.98	168.01 to 148.05	L Stemmann, M Picheral
uvp5_sn003_ccelter_2014	42	62	2014-08-07 to 2014-09-02	34.87 to 32.28	-118.28 to -123.9	L Stemmann, M Picheral
uvp5_sn003_ccelter_2014	42	62	2014-08-07 to 2014-09-02	34.87 to 32.28	-118.28 to -123.9	L Stemmann, M Picheral
uvp5_sn003_ccelter_2016	43	60	2016-04-20 to 2016-05-11	35.09 to 32.7	-117.36 to -123.21	T Biard
uvp5_sn003_csiro_iioe	144	52	2019-05-15 to 2019-06-09	-11.45 to -39.49	113.42 to 109.88	D Antoine
uvp5_sn003_dewex_spring_2013	44	83	2013-04-05 to 2013-04-19	43.63 to 40.08	8.64 to 3.51	L Stemmann, M Picheral
uvp5_sn003_iado_2017	90	24	2017-09-22 to 2017-09-24	43.67 to 43.35	7.65 to 7.31	J-O Irisson
uvp5_sn003_jerico_2017	1	27	2017-07-10 to 2017-07-16	59.85 to 54.97	24.84 to 10.5	L Stemmann, M Picheral
uvp5_sn003_mobydick_2018	124	61	2018-02-21 to 2018-03-19	-29.04 to -52.6	74.9 to 59.06	L Guidi
uvp5_sn003_outpace_2015	46	205	2015-02-21 to 2015-03-31	-17.9 to -22.0	178.64 to -178.51	L Guidi
uvp5_sn003_sargasso_a	47	52	2014-03-16 to 2014-04-05	31.5 to 24.67	-62.48 to -68.56	F Lombard
uvp5_sn003_sargasso_b	48	32	2014-04-09 to 2014-04-22	35.18 to 25.67	-31.63 to -59.52	F Lombard
uvp5_sn003_tara2013	49	155	2013-05-26 to 2013-10-27	79.67 to 54.41	174.99 to -168.66	L Stemmann, M Picheral
uvp5_sn003zp_pelgas2012	50	34	2012-05-26 to 2012-06-03	46.11 to 44.86	-1.27 to -2.6	L Stemmann, M Picheral
uvp5_sn003zp_tara2012	51	77	2011-12-30 to 2012-03-26	44.36 to 9.84	-10.07 to -88.49	L Stemmann, M Picheral
uvp5_sn005_batman	52	6	2016-03-11 to 2016-03-15	42.8 to 42.8	6.08 to 6.08	F Carlotti, Leo Berline
uvp5_sn005_dewex_2013_winter	53	53	2013-02-03 to 2013-02-18	42.88 to 40.08	8.59 to 3.45	L Stemmann, M Picheral
uvp5_sn005_dy032_2015_filtered	54	15	2015-06-24 to 2015-07-03	49.08 to 48.68	-16.26 to -17.06	F Carlotti, Leo Berline
uvp5_sn005_moose_ge_2013	55	39	2013-06-29 to 2013-07-07	43.05 to 39.96	8.0 to 3.39	L Stemmann, M Picheral
UVPsn008_2018_leg02c	152	42	2018-07-25 to 2018-08-13	71.41 to 59.22	-48.46 to -70.18	M Babin, M Picheral
uvp5_sn008_an1304	56	101	2013-07-29 to 2013-09-15	81.28 to 53.8	-55.43 to -116.96	M Babin, M Picheral
uvp5_sn008_an1405	57	64	2014-07-27 to 2014-08-13	81.37 to 68.68	-57.88 to -108.51	M Babin, M Picheral
uvp5_sn008_an1406	58	82	2014-08-17 to 2014-09-23	75.21 to 69.37	-123.03 to -169.83	M Babin, M Picheral
uvp5_sn008_an1407	59	11	2014-09-30 to 2014-10-08	71.12 to 53.8	-55.44 to -72.26	M Babin, M Picheral

uvp5_sn008_green_2015_icecamp	60	32	2015-04-18 to 2015-06-21	67.48 to 67.48	-63.79 to -63.79	M Babin, M Picheral
uvp5_sn008_green_2016_icecamp	61	29	2016-03-02 to 2016-07-04	67.48 to 67.48	-63.79 to -63.79	M Babin, M Picheral
uvp5_sn008_ips_amundsen_2018	105	7	2018-07-16 to 2018-07-22	69.29 to 67.24	-60.39 to -64.64	M Babin, M Picheral
uvp5_sn008_subice_2014	62	228	2014-05-15 to 2014-06-20	73.27 to 63.95	-162.0 to -168.95	L Stemmann, M Picheral
uvp5_sn008_uvp_azomp	161	35	2019-06-01 to 2019-06-17	60.57 to 44.27	-48.23 to -63.32	
uvp5_sn009_pomz	132	29	2016-12-27 to 2017-01-13	21.36 to 14.0	-104.63 to -107.83	A.M.P. McDonnell
uvp5_sn009_en_534_mcdonnell	257	10	2013-10-24 to 2013-10-27	39.81 to 38.38	-71.01 to -72.91	A.M.P. McDonnell
uvp5_sn009_2015_goa	63	70	2015-07-17 to 2015-07-30	60.3 to 54.64	-132.86 to -149.47	A.M.P. McDonnell, J.S. Turner
uvp5_sn009_2015_p16n	64	171	2015-04-11 to 2015-06-18	56.29 to -16.96	-149.86 to -153.23	A.M.P. McDonnell
uvp5_sn009_2015_p16n_goa	65	15	2015-06-19 to 2015-06-23	56.79 to 54.35	-135.95 to -149.14	A.M.P. McDonnell, J.S. Turner
uvp5_sn009_2016_goa_fall	146	37	2016-09-16 to 2016-09-21	61.08 to 57.8	-146.75 to -149.48	A.M.P. McDonnell
uvp5_sn009_2016_goa_spring	141	33	2016-04-30 to 2016-05-27	60.99 to 57.79	-147.08 to -149.49	A.M.P. McDonnell
uvp5_sn009_2017_asgard	112	71	2017-06-09 to 2017-06-27	69.04 to 63.3	-164.43 to -172.59	A.M.P. McDonnell
uvp5_sn009_2017_sewardline_fall	142	49	2017-09-16 to 2017-09-22	60.99 to 57.79	-146.98 to -149.49	A.M.P. McDonnell
uvp5_sn009_2018_asgard_filtered	234	69	2018-06-06 to 2018-06-24	69.45 to 61.29	-164.43 to -171.51	A.M.P. McDonnell
uvp5_sn009_2018_nga_fall_filtered	131	60	2018-09-12 to 2018-09-21	60.25 to 57.21	-145.5 to -151.39	A.M.P. McDonnell
uvp5_sn009_2019_nga_lter_spring_filtered	139	54	2019-04-30 to 2019-05-08	60.83 to 56.97	-147.39 to -151.58	A.M.P. McDonnell
uvp5_sn009_2019_nga_lter_summer_filtered	151	57	2019-06-29 to 2019-07-17	60.53 to 56.66	-144.59 to -151.59	A.M.P. McDonnell
uvp5_sn009_2019_nga_lter_summer_filtered	151	57	2019-06-29 to 2019-07-17	60.53 to 56.66	-144.59 to -151.59	A.M.P. McDonnell
uvp5_sn009_chukchi_borderlands_2016	147	21	2016-07-08 to 2016-08-02	78.35 to 71.6	-158.48 to -164.06	A.M.P. McDonnell
uvp5_sn009_2018_nga_spring_filtered	104	70	2018-04-19 to 2018-05-04	61.25 to 57.79	-143.89 to -149.47	A.M.P. McDonnell
uvp5_sn009_sewardline_f2014	66	10	2014-09-13 to 2014-09-16	59.84 to 58.24	-147.93 to -149.49	A.M.P. McDonnell
uvp5_sn009_tb14	148	24	2014-08-20 to 2014-08-28	70.62 to 69.72	-140.3 to -145.11	A.M.P. McDonnell
uvp5_sn009_txs14	67	9	2014-05-03 to 2014-05-05	59.84 to 58.68	-148.35 to -149.48	A.M.P. McDonnell
uvp5_sn010_2014_eddy	109	6	2014-02-14 to 2014-03-07	19.51 to 16.75	-24.3 to -25.12	R Kiko, H Hauss
uvp5_sn010_2014_m105	68	138	2014-03-18 to 2014-04-14	19.23 to 7.0	-17.5 to -26.0	R Kiko, H Hauss
uvp5_sn010_2014_m106	69	115	2014-04-19 to 2014-05-24	17.6 to -11.5	-21.21 to -35.89	R Kiko, H Hauss
uvp5_sn010_2014_m107	70	73	2014-06-05 to 2014-06-29	19.9 to 11.45	-16.32 to -23.0	R Kiko, H Hauss
uvp5_sn010_2014_m108	71	12	2014-07-09 to 2014-07-20	49.0 to 39.52	-15.96 to -16.52	R Kiko
uvp5_sn010_2014_ps88b	72	39	2014-11-04 to 2014-11-15	21.21 to -1.0	-21.12 to -24.29	R Kiko, H Hauss
uvp5_sn010_2015_m116	73	82	2015-05-02 to 2015-06-02	17.58 to 5.0	-18.0 to -57.67	R Kiko, H Hauss
uvp5_sn010_2015_m119	74	49	2015-09-08 to 2015-09-26	17.61 to -5.0	-21.21 to -24.33	R Kiko, H Hauss
uvp5_sn010_2015_m120	75	8	2015-10-31 to 2015-11-02	-6.21 to -10.59	13.43 to 11.38	R Kiko, H Hauss
uvp5_sn010_2015_m121	76	88	2015-11-22 to 2015-12-24	-3.0 to -29.58	15.56 to -0.01	R Kiko, H Hauss
uvp5_sn010_2016_love	226	43	2016-03-30 to 2016-04-07	68.27 to 67.78	14.7 to 14.04	H Hauss, R Kiko
uvp5_sn010_2016_m130	77	112	2016-08-29 to 2016-10-01	17.7 to -11.5	-19.0 to -35.89	R Kiko, H Hauss
uvp5_sn010_2016_m131	223	89	2016-10-08 to 2016-11-09	-6.21 to -23.0	14.37 to -32.0	R Kiko, H Hauss
uvp5_sn010_2017_fluxes1	110	72	2017-07-14 to 2017-08-08	23.0 to 17.5	-17.64 to -26.0	R Kiko

uvp5_sn010_2017_fluxes2	111	53	2017-11-02 to 2017-11-20	27.67 to 20.39	-15.82 to -20.65	R Kiko
uvp5_sn010_2017_m135	95	141	2017-03-02 to 2017-04-07	-10.67 to -31.03	-70.3 to -86.0	R Kiko, H Hauss
uvp5_sn010_2017_m136	96	98	2017-04-12 to 2017-05-02	-12.19 to -15.51	-76.47 to -78.5	R Kiko, H Hauss
uvp5_sn010_2017_m137	97	85	2017-05-06 to 2017-05-27	-12.1 to -12.98	-77.06 to -78.19	R Kiko, H Hauss
uvp5_sn010_2017_m138	98	42	2017-06-03 to 2017-06-29	1.5 to -16.25	-75.43 to -85.84	R Kiko, H Hauss
uvp5_sn010_2018_m145	172	89	2018-02-13 to 2018-03-12	17.61 to -11.5	-21.23 to -35.89	R Kiko, H Hauss
uvp5_sn010_2018_m147	171	4	2018-05-01 to 2018-05-04	3.95 to 1.91	-46.44 to -48.26	R Kiko, H Hauss
uvp5_sn010_2018_m148	173	92	2018-05-30 to 2018-06-28	-6.21 to -22.67	14.21 to -35.88	R Kiko, H Hauss
uvp5_sn011_2016_syTUMSAT1	246	2	2016-09-26 to 2016-09-27	35.06 to 35.06	138.78 to 138.68	Y. Tanaka
uvp5_sn011_2017_syTUMSAT2	247	10	2017-05-22 to 2017-05-24	35.1 to 33.4	139.87 to 139.41	Y. Tanaka
uvp5_sn200_ilhas_2017_filtered	240	38	2017-02-02 to 2017-02-13	-20.06 to -21.14	-28.3 to -40.25	R. Lopes
uvp5_sn200_moose_ge_2018_filtered	168	32	2018-05-27 to 2018-06-05	43.0 to 40.0	7.98 to 3.82	L Coppola
uvp5_sn200_perle_02_2019_filtered	235	31	2019-02-27 to 2019-03-04	35.95 to 34.04	25.3 to 22.96	X. D. de Madron
uvp5_sn200_perle_02_2019_filtered	235	31	2019-02-27 to 2019-03-04	35.95 to 34.04	25.3 to 22.96	X. D. de Madron
uvp5_sn201_2015_naames_01	80	26	2015-11-14 to 2015-11-25	54.11 to 40.51	-37.51 to -40.48	L. Karp-Boss, E. Boss
uvp5_sn201_2016_naames_02	81	42	2016-05-17 to 2016-05-29	56.34 to 44.05	-38.21 to -46.15	L. Karp-Boss, E. Boss
uvp5_sn201_2017_naames_03	92	40	2017-09-04 to 2017-09-17	53.4 to 42.38	-39.13 to -48.95	L. Karp-Boss, E. Boss
uvp5_sn201_2018_naames_04_filtered	236	12	2018-03-27 to 2018-04-01	44.48 to 39.28	-38.28 to -43.53	L. Karp-Boss, E. Boss
uvp5_sn201_ccelter_2017	83	90	2017-06-01 to 2017-07-01	35.58 to 33.02	-118.11 to -123.18	T Biard
uvp5_sn201_ccelter_2019_filtered	154	77	2019-08-06 to 2019-09-05	36.45 to 32.86	-117.66 to -125.07	T Biard
uvp5_sn201_exports01_filtered	228	84	2018-08-14 to 2018-09-09	50.6 to 49.93	-144.35 to -145.22	L. Karp-Boss, E. Boss
uvp5_sn202_msm060_filtered	231	127	2017-01-04 to 2017-01-31	-34.04 to -34.83	18.15 to -51.83	A. Rogge
uvp5_sn202_msm074_filtered	232	114	2018-05-25 to 2018-06-19	60.4 to 47.55	-36.1 to -54.0	A. Rogge
uvp5_sn202_ps99_20_06_filtered	237	8	2016-06-20 to 2016-06-20	74.93 to 74.7	18.15 to 17.36	A. Rogge
uvp5_sn202_ps99_21_06_3_filtered	85	27	2016-06-22 to 2016-07-12	79.59 to 77.59	11.09 to -5.41	A. Rogge
uvp5_sn203_greenedge_2016	86	86	2016-06-05 to 2016-06-22	69.03 to 50.34	-52.84 to -63.2	L. Stemmann, M. Picheral
uvp5_sn203_greenedge_2016_1b	87	110	2016-06-24 to 2016-07-10	70.51 to 68.02	-56.9 to -63.28	L. Stemmann, M. Picheral
uvp5_sn205_coastdark_2019	153	38	2019-07-26 to 2019-08-11	79.04 to 76.64	16.87 to 7.76	E. Trudnowska
uvp5_sn205_perle_02_2019_filtered	134	81	2019-03-04 to 2019-03-16	35.88 to 33.54	28.81 to 24.38	X. D. de Madron
uvp5_sn205_perle_03_2020_filtered	238	21	2020-03-13 to 2020-03-16	42.94 to 39.19	14.26 to 9.59	X. D. de Madron
uvp5_sn207_2018_exports_np_sr1812_filtered	230	134	2018-08-11 to 2018-09-09	51.04 to 49.43	-131.54 to -145.76	A.M.P. McDonnell
uvp5_sn207_2018_s04p_filtered	150	111	2018-03-13 to 2018-05-09	-59.06 to -75.29	179.42 to -179.29	A.M.P. McDonnell
uvp5hd_sn207_2019_i06s_tcn322_filtered	138	44	2019-04-16 to 2019-05-11	-33.23 to -68.35	31.53 to 28.09	A.M.P. McDonnell
uvp5_sn210_2018_msm080	270	127	2018-12-27 to 2019-01-25	-8.5 to -16.4	-74.17 to -81.0	R Kiko, H Hauss
uvp5_sn210_2019_m156	271	57	2019-07-04 to 2019-07-29	21.44 to 17.58	-16.39 to -24.33	R Kiko, H Hauss
uvp5_sn210_2019_m157	272	24	2019-08-21 to 2019-09-13	-17.26 to -25.0	14.56 to 11.07	R Kiko, H Hauss
uvp5_sn210_2019_m159	256	46	2019-11-02 to 2019-11-18	17.6 to -11.5	-24.25 to -35.02	R Kiko, H Hauss
uvp5_sn210_2019_m160	275	71	2019-11-24 to 2019-12-17	18.6 to 14.27	-19.7 to -25.99	R Kiko, H Hauss

uvp5_sn210_2020_msm089	273	46	2020-01-18 to 2020-02-16	14.03 to 7.25	-50.83 to -60.08	R Kiko, H Hauss
uvp5_sn221_algoa_bay_2020	268	36	2020-10-28 to 2020-11-23	-33.73 to -34.03	26.29 to 25.7	Margaux Noyon

Table 2

Table 2: References for datasets published before the revision of the inter-calibration procedure.

UVP project name	Link to previously published UVP particle dataset
uvp5_sn000_tara2009	https://doi.pangaea.de/10.1594/PANGAEA.836321
uvp5_sn000_tara2010	https://doi.pangaea.de/10.1594/PANGAEA.836321
uvp5_sn000_tara2011	https://doi.pangaea.de/10.1594/PANGAEA.836321
uvp5_sn000_tara2012	https://doi.pangaea.de/10.1594/PANGAEA.836321
uvp5_sn003_tara2013	https://doi.pangaea.de/10.1594/PANGAEA.836321
uvp5_sn003zp_tara2012	https://doi.pangaea.de/10.1594/PANGAEA.836321
uvp5_sn001_2012_msm22	https://doi.org/10.1594/PANGAEA.874871
uvp5_sn001_2012_msm23	https://doi.pangaea.de/10.1594/PANGAEA.846229
uvp5_sn001_2013_m92	https://doi.org/10.1594/PANGAEA.885756
uvp5_sn001_2013_m96	https://doi.pangaea.de/10.1594/PANGAEA.846153
uvp5_sn010_2014_m106	https://doi.org/10.1594/PANGAEA.874870
uvp5_sn010_2014_m107	https://doi.org/10.1594/PANGAEA.885759
uvp5_sn010_2015_m119	https://doi.org/10.1594/PANGAEA.874872
uvp5_sn003_cassiopee_2015	https://doi.org/10.1594/PANGAEA.876216
uvp5_sn009_2015_p16n	https://doi.org/10.1594/PANGAEA.874875
uvp5_sn202_ps99_21_06_3_filtered	https://doi.pangaea.de/10.1594/PANGAEA.896047

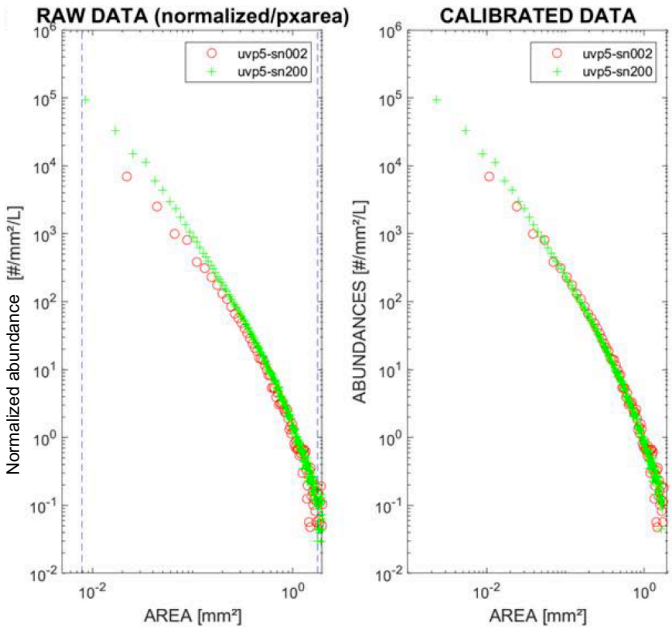

Figure 1. UVP5 inter-calibration procedure based on the normalized size spectrum. To calculate the normalized size spectrum, the abundance of particles in a given size class is divided by the mean area of the size class. Normalized abundance of each size class is then plotted against the area of the size class. Figure 1a shows the raw number size spectrum data of the unit to be adjusted (sn200) for one exemplary inter-calibration experiment against sn002 and Fig 1b the respective data after adjustment of the parameters Aa and Exp to coincide better with the number size spectrum of UVP5 sn002.

Figures

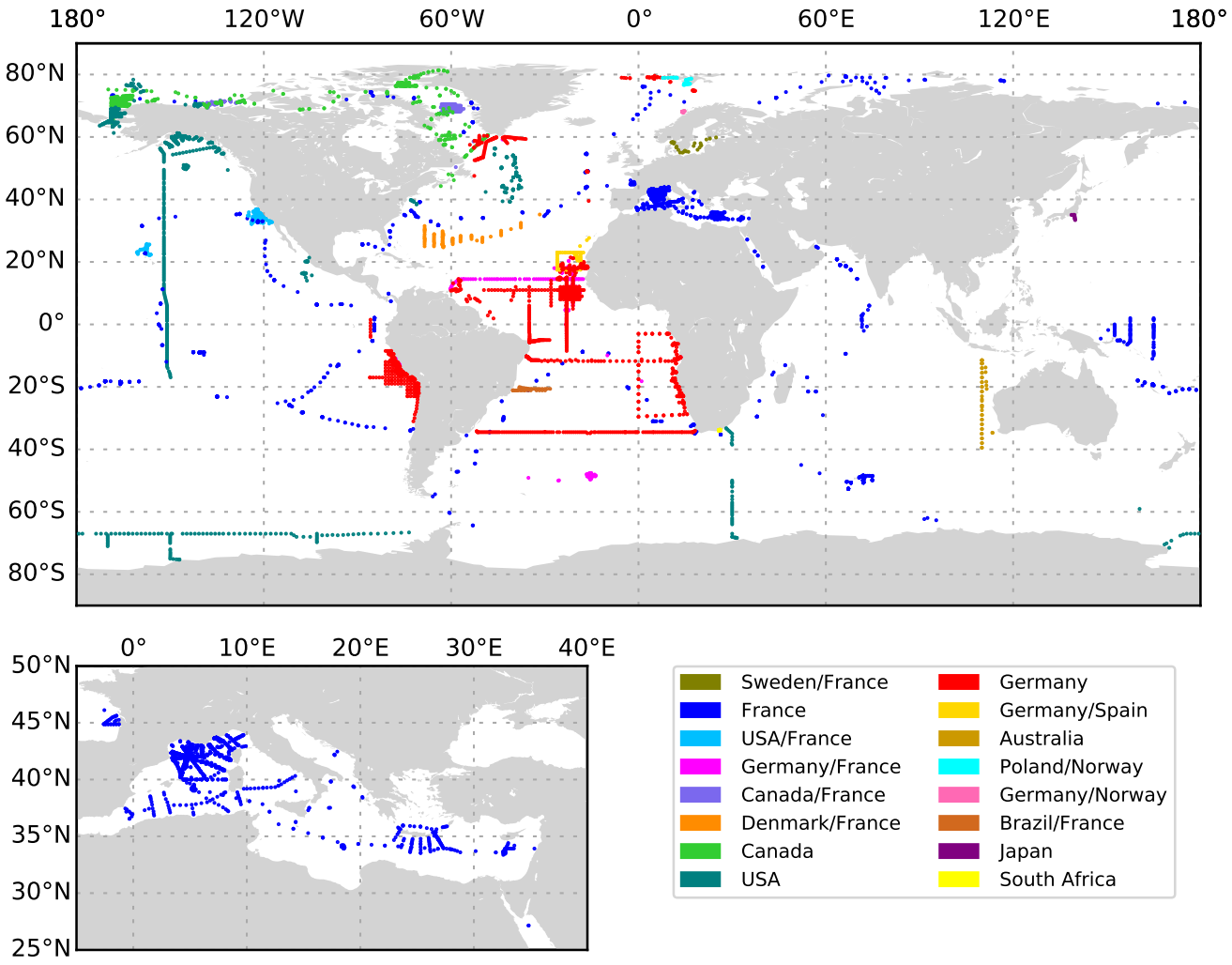

Figure 2. Global distribution of UVP5 data. Lower left panel shows the data distribution in the Mediterranean Sea.

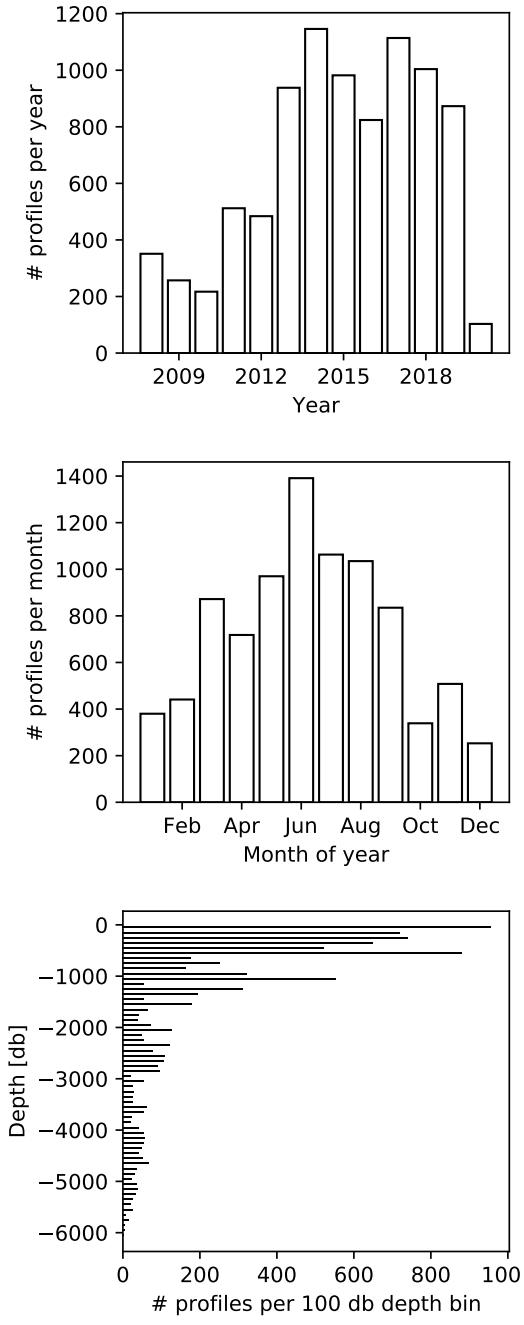

Figure 3. UVP5 data distribution per year, month and maximum profile depth (aggregated in 100 dbar depth bins).

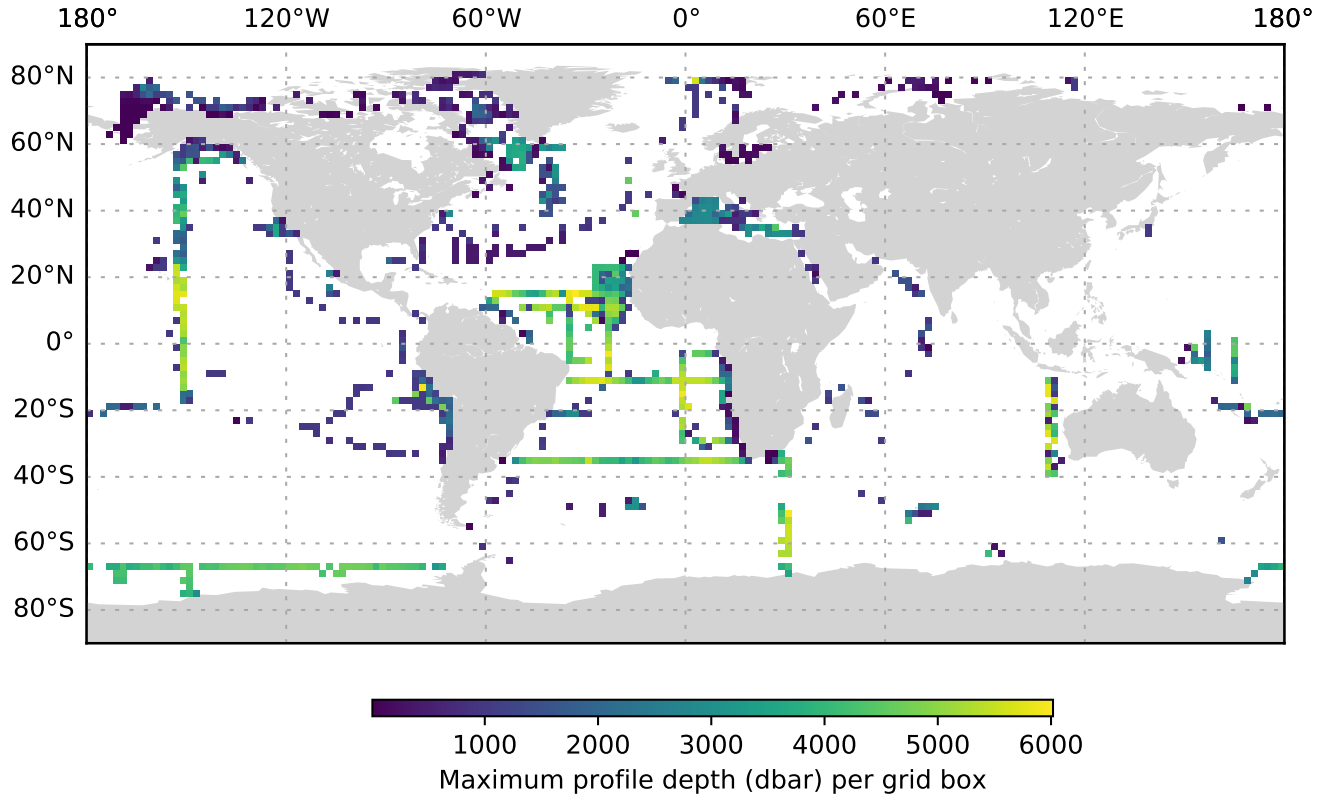

Figure 4. Maximum UVP5 profile depth per two degree grid box.

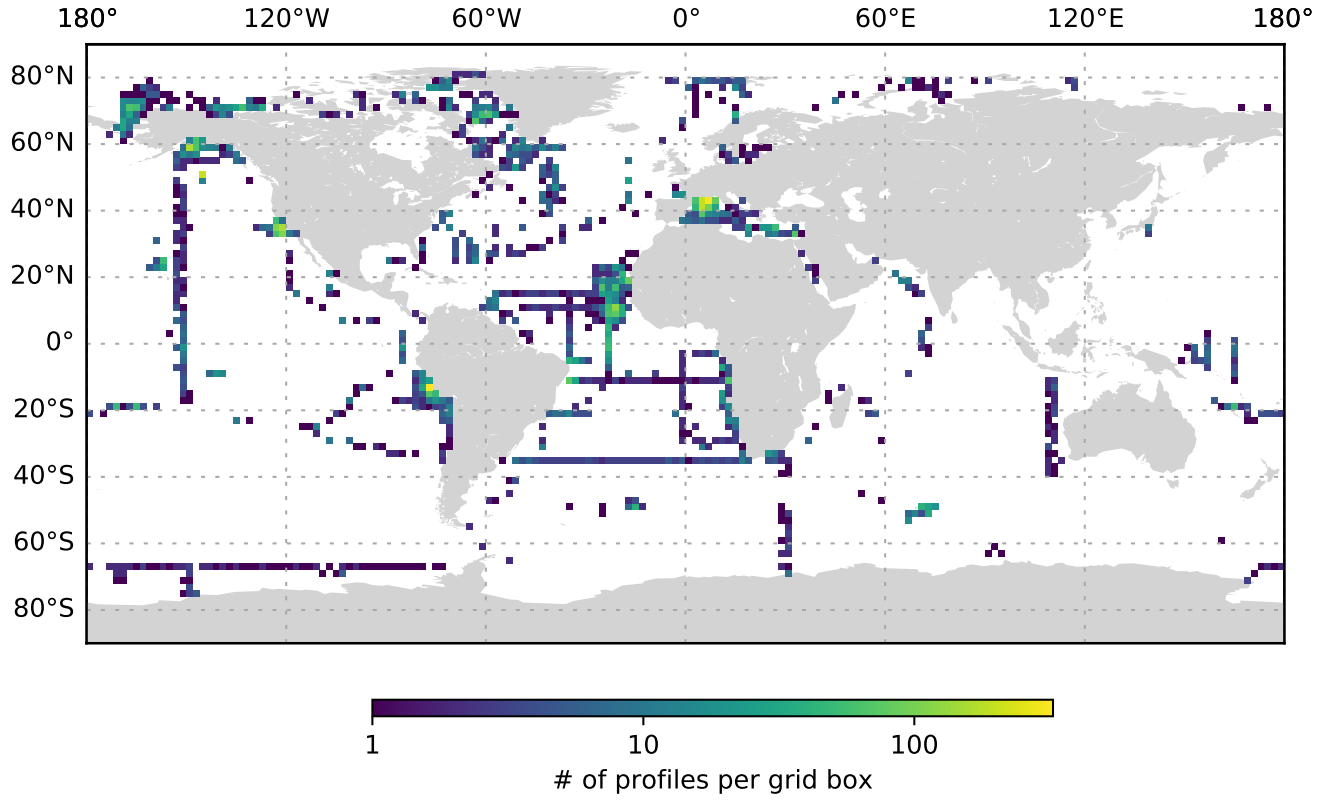

Figure 5. UVP5 data distribution per two degree grid box.

Figure 6.

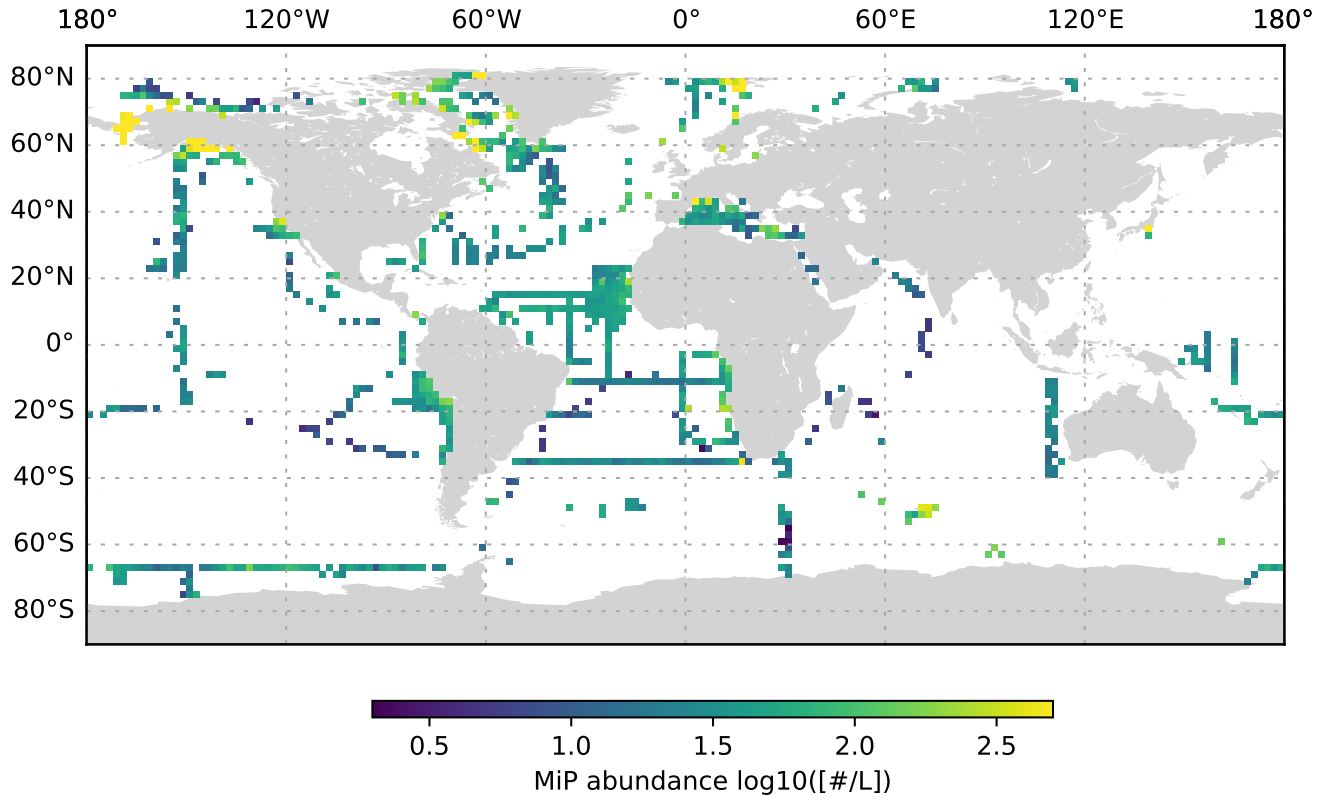

MiP abundance (decadic logarithm) averaged for the 0 to 200 dbar depth layer and per 2 degree grid box. Only profiles at least 200 dbar deep were used for the analysis.

Figure 7.

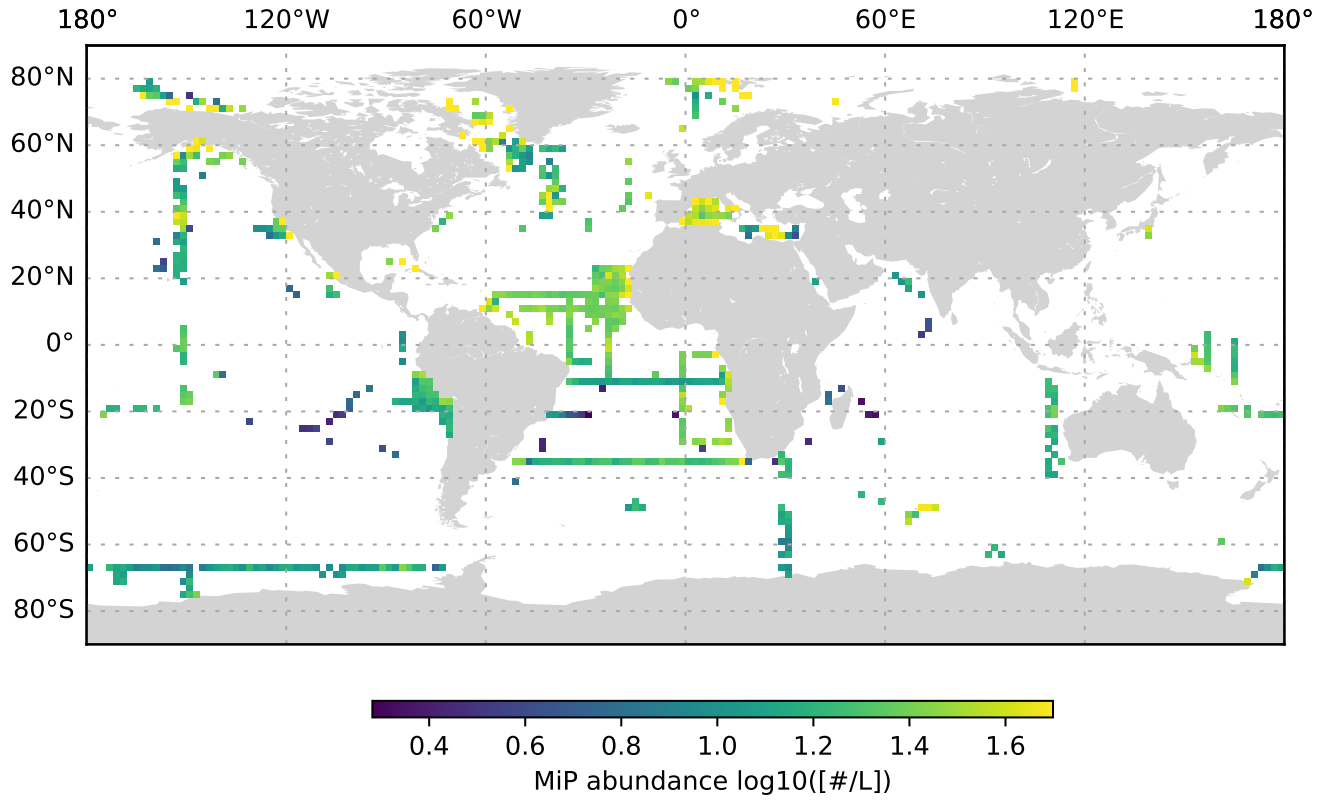

MiP abundance (decadic logarithm) averaged for the 200 to 1000 dbar depth layer and per 2 degree grid box. Only profiles at least 1000 dbar deep were used for the analysis.

Figure 8.

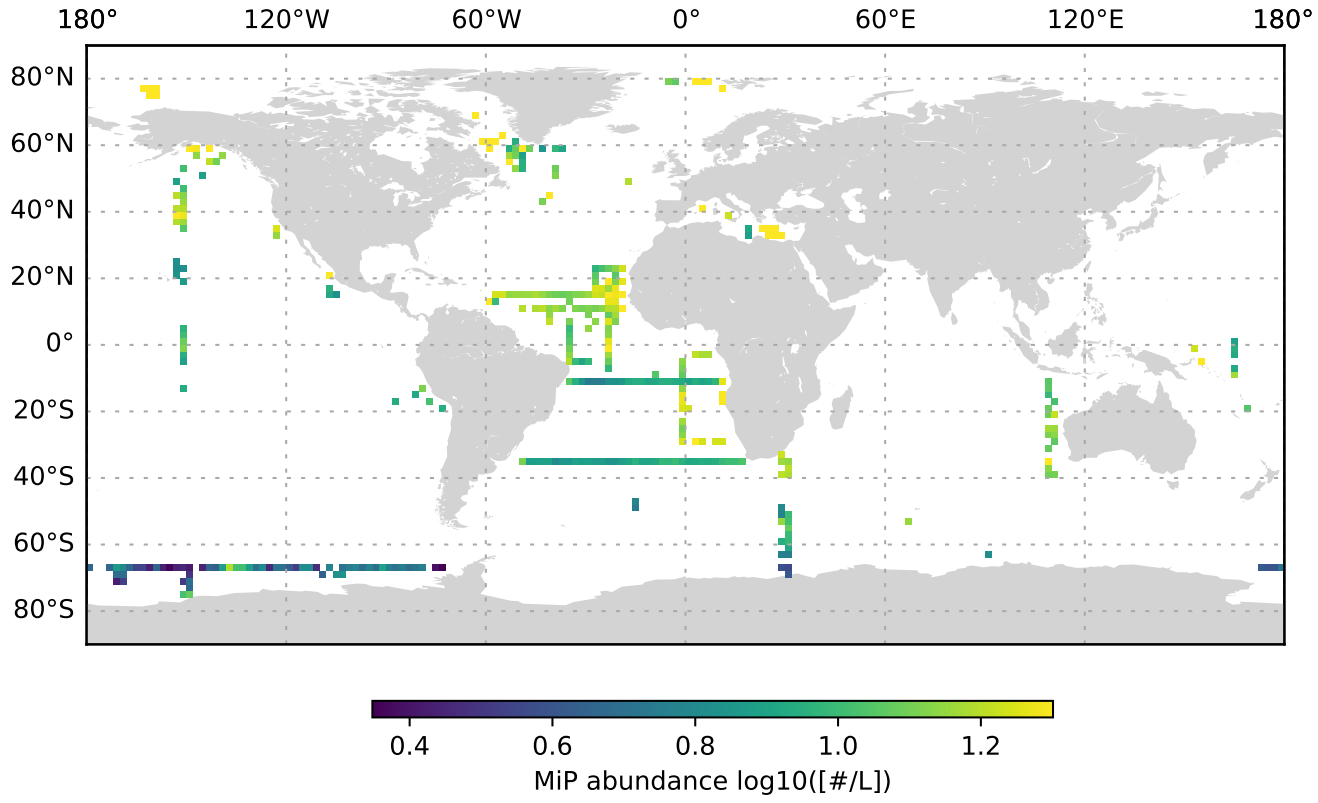

MiP abundance (decadic logarithm) averaged for the 1000 to 3000 dbar depth layer and per 2 degree grid box. Only profiles at least 3000 dbar deep were used for the analysis.

Figure 9.

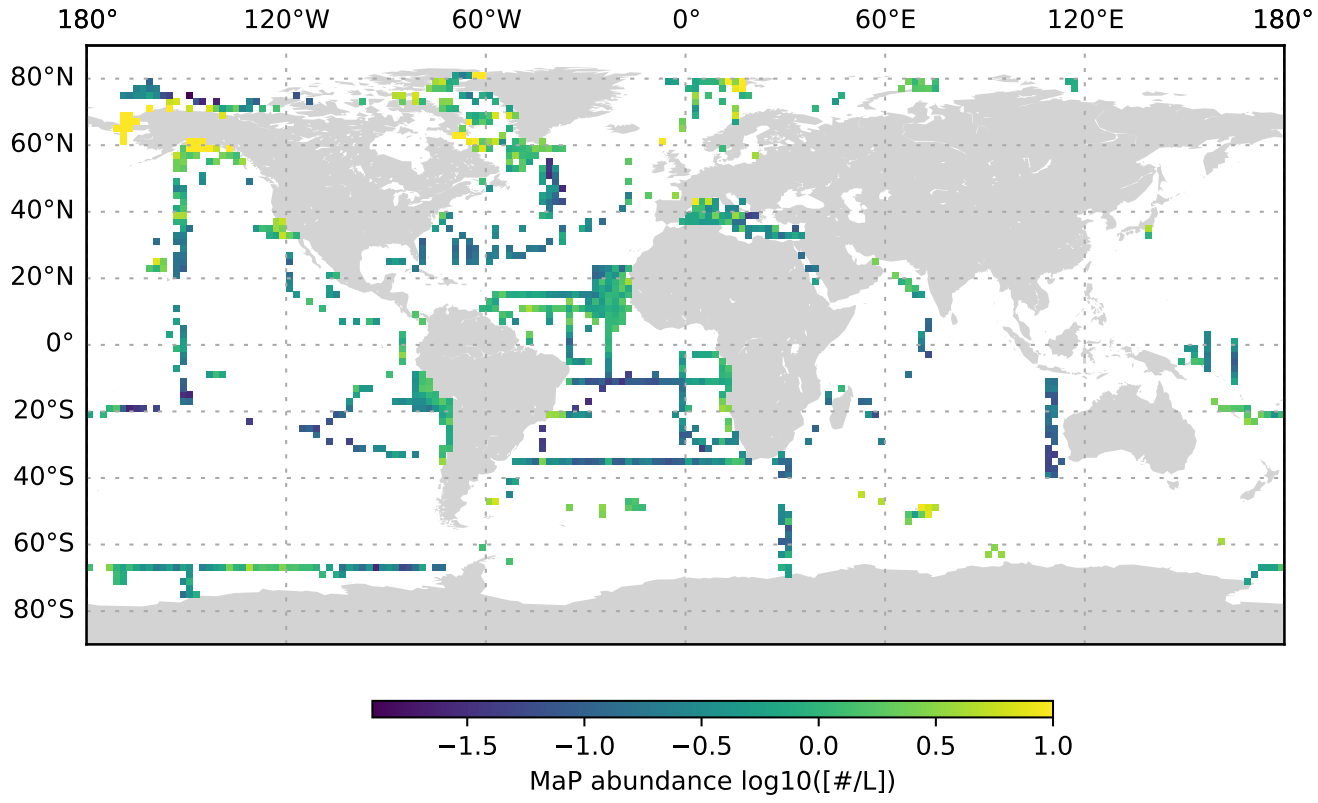

MaP abundance (decadic logarithm) averaged for the 0 to 200 dbar depth layer and per 2 degree grid box. Only profiles at least 200 dbar deep were used for the analysis.

Figure 10.

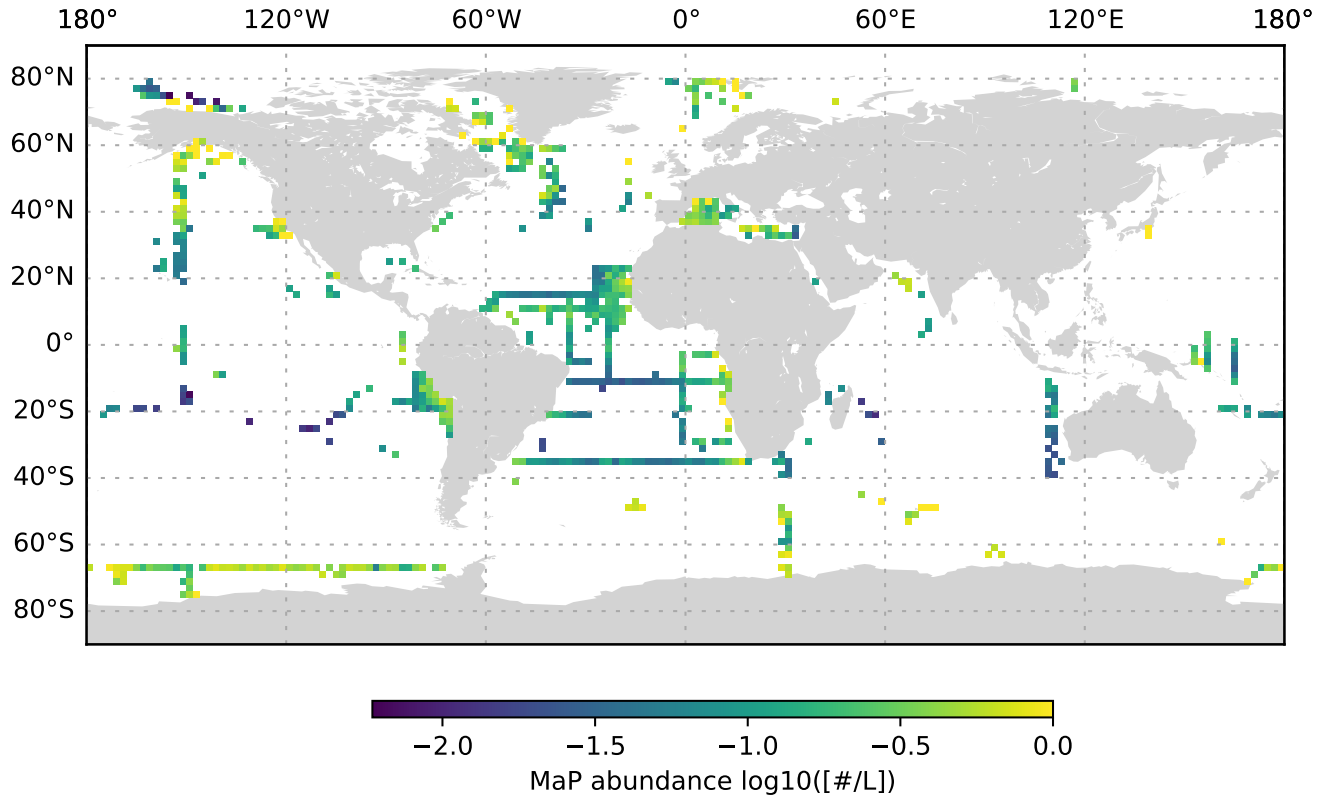

MaP abundance (decadic logarithm) averaged for the 200 to 1000 dbar depth layer and per 2 degree grid box. Only profiles at least 1000 dbar deep were used for the analysis.

Figure 11.

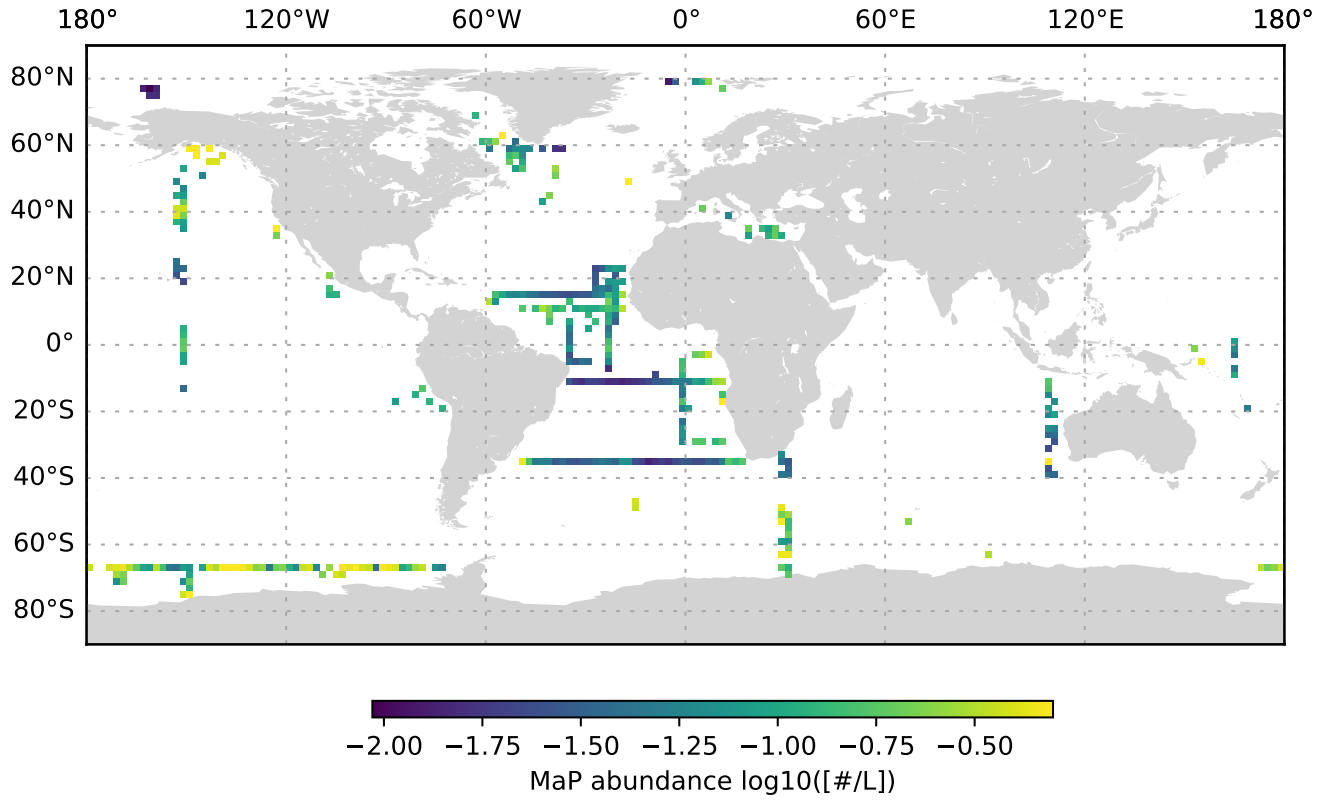

MaP abundance (decadic logarithm) averaged for the 1000 to 3000 dbar depth layer and per 2 degree grid box. Only profiles at least 3000 dbar deep were used for the analysis.

Figure 12.

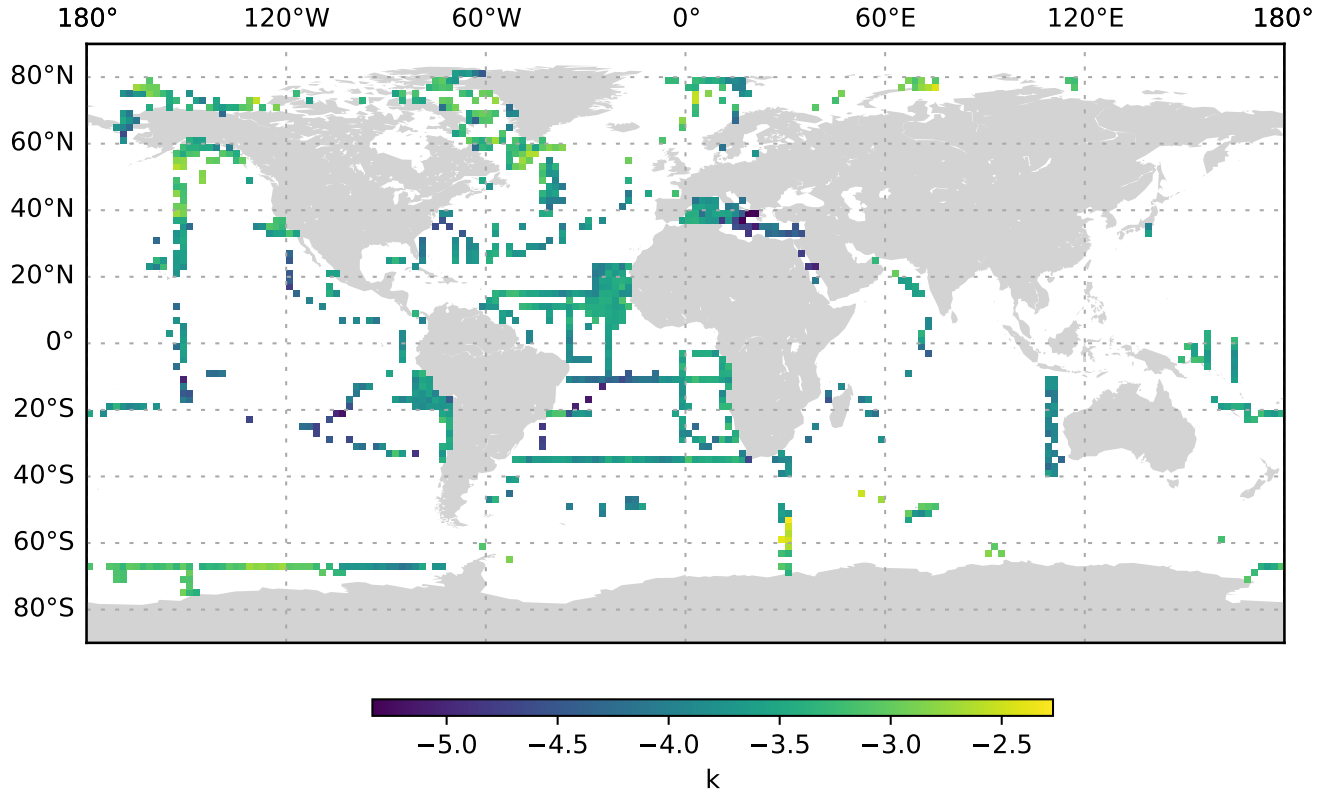

k averaged for the 0 to 200 dbar depth layer and per 2 degree grid box. Only profiles at least 200 dbar deep were used for the analysis.

Figure 13.

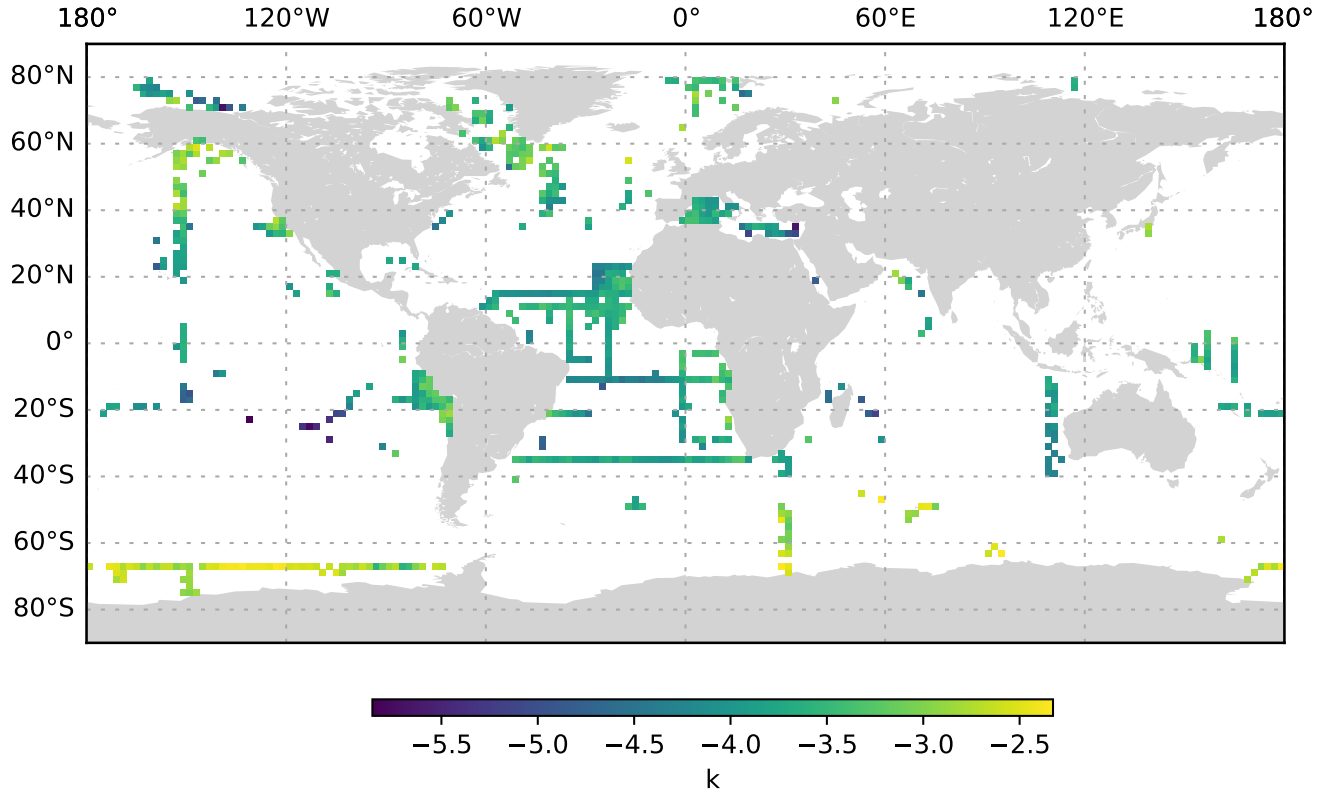

k averaged for the 200 to 1000 dbar depth layer and per 2 degree grid box. Only profiles at least 1000 dbar deep were used for the analysis.

Figure 14.

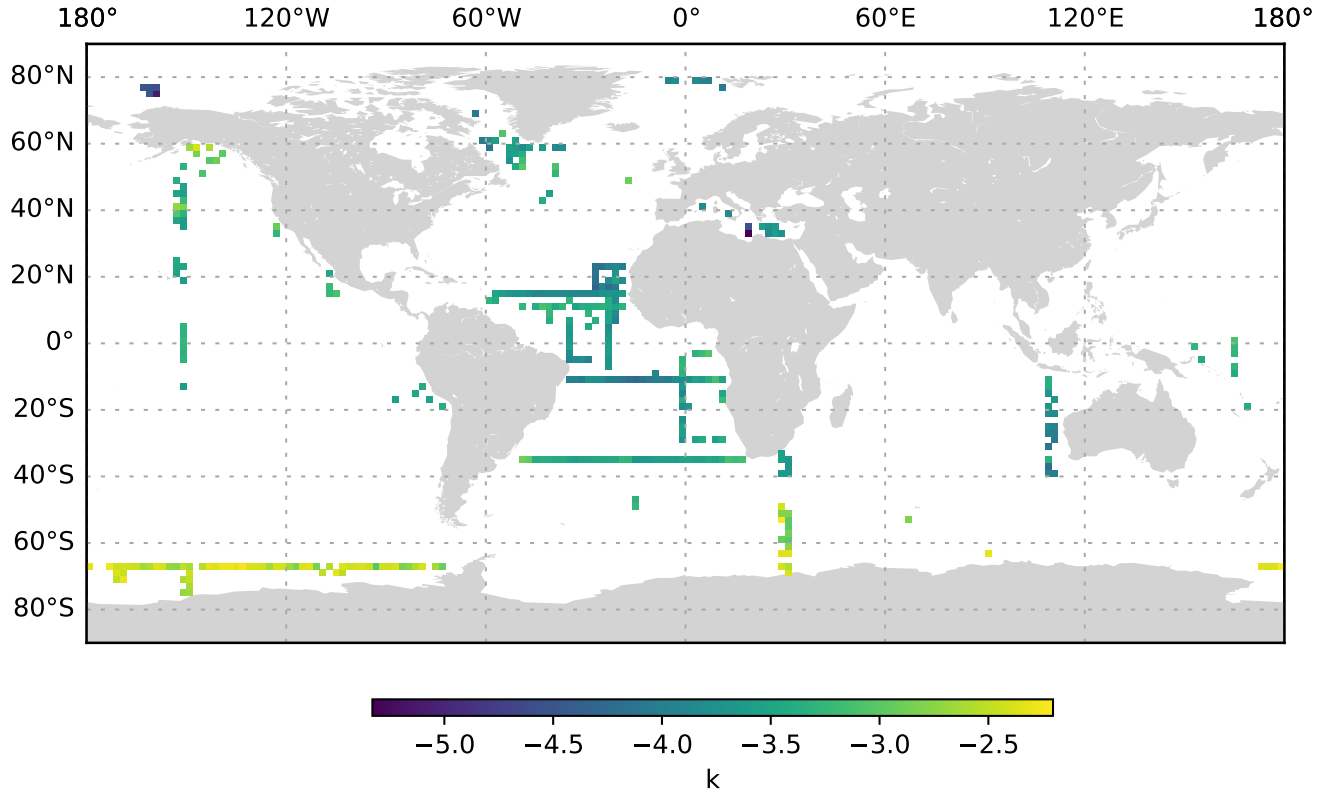

k averaged for the 1000 to 3000 dbar depth layer and per 2 degree grid box. Only profiles at least 3000 dbar deep were used for the analysis.